AD-A114 983 NAVAL RESEARCH LAB. WASHINGTON DC F/G 12/1
THE USE OF FINITE J SUB THETA FOR INCREASING THE ION EFFICIENCY--ETC(U)
APR 82 R J BARKER, S A GOLDSTEIN
UNCLASSIFIED NRL-MR-4773 NL

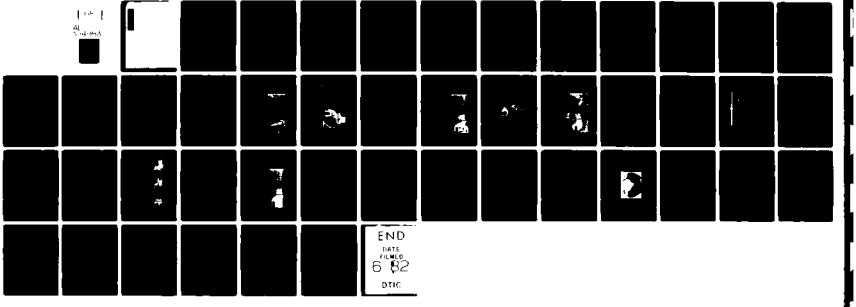

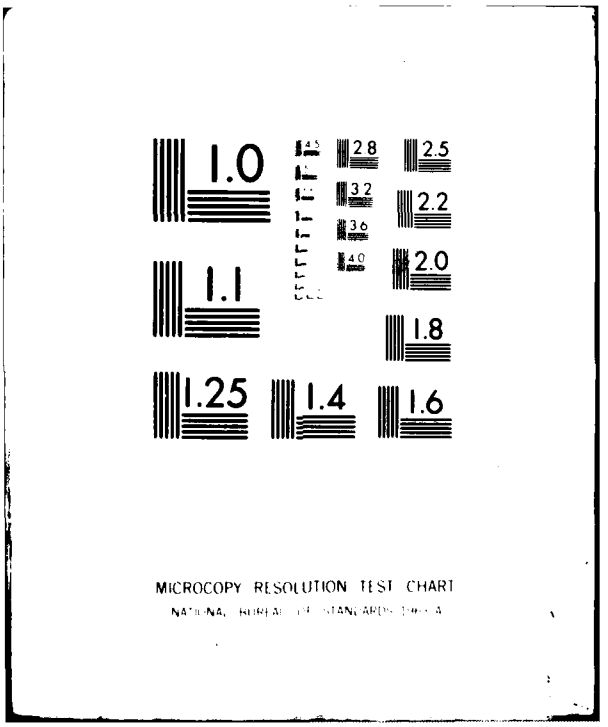
1.0
1.1
1.25
1.4
1.6
1.8
2.0
2.2
2.5
2.8
3.2
3.6
4.0
MICROCOPY RESOLUTION TEST CHART

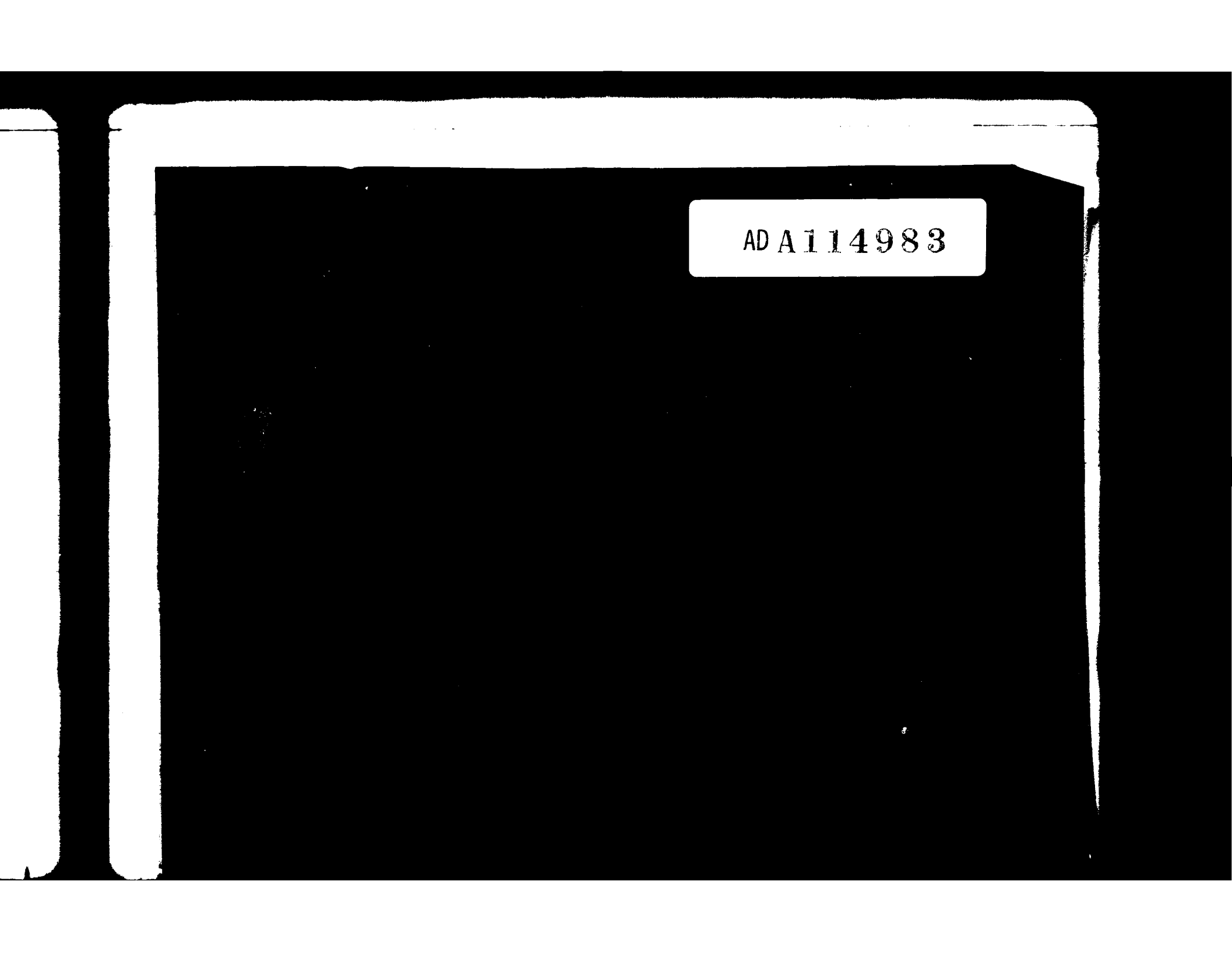
AD A114983

SECURITY CLASSIFICATION OF THIS PAGE (When Data Entered)

REPORT DOCUMENTATION PAGE		READ INSTRUCTIONS BEFORE COMPLETING FORM
1. REPORT NUMBER NRL Memorandum Report 4773	2. GOVT ACCESSION NO. AD-A114 983	3. RECIPIENT'S CATALOG NUMBER
4. TITLE (and Subtitle) THE USE OF FINITE J_θ FOR INCREASING THE ION EFFICIENCY OF HIGH IMPEDANCE DIODES		5. TYPE OF REPORT & PERIOD COVERED Interim report on a continuing NRL problem 6. PERFORMING ORG. REPORT NUMBER
7. AUTHOR(s) Robert J. Barker* and Shyke A. Goldstein*		8. CONTRACT OR GRANT NUMBER(s)
9. PERFORMING ORGANIZATION NAME AND ADDRESS Naval Research Laboratory Washington, DC 20375		10. PROGRAM ELEMENT, PROJECT, TASK AREA & WORK UNIT NUMBERS T99QAXLA014 NRL Problem 47-0875-0-1 NRL Problem 47-0879-0-1
11. CONTROLLING OFFICE NAME AND ADDRESS Defense Nuclear Agency, Washington, DC 20305 Department of Energy, Washington, DC 20545		12. REPORT DATE April 12, 1982 13. NUMBER OF PAGES 45
14. MONITORING AGENCY NAME & ADDRESS(if different from Controlling Office)		15. SECURITY CLASS. (of this report) UNCLASSIFIED 15a. DECLASSIFICATION/DOWNGRADING SCHEDULE

16. DISTRIBUTION STATEMENT (of this Report)

Approved for public release, distribution unlimited.

17. DISTRIBUTION STATEMENT (of the abstract entered in Block 20, if different from Report)

18. SUPPLEMENTARY NOTES

*Present Address: Jaycor Inc., 205 S. Whiting St., Alexandria, VA 22305

This research was sponsored in part by the Defense Nuclear Agency under Subtask T99QAXLA014, work unit 46 and work unit title "Ion Beam Generation" and by the Department of Energy, Washington, D.C.

19. KEY WORDS (Continue on reverse side if necessary and identify by block number)

Numerical simulation
Intense ion beams
Magnetic insulation
Pinch-reflex diode

20. ABSTRACT (Continue on reverse side if necessary and identify by block number)

Numerical simulations predict that the ratio of the effective ion current to total diode current can be significantly increased by introducing a small but finite azimuthal current into the tip of the cathode shank of a high impedance (4 Ω) axial pinch-reflex diode. Such a current generates large tangential magnetic fields along the electron-emitting cathode surfaces. These fields, in turn, impart a finite angular momentum to the electrons as they are injected into the anode-cathode gap. The resultant particle self-fields alter electron trajectories in such a way as to boost electron space charge near certain portions of the ion-emitting anode surface. The net consequence is a modification

(Continued)

DD FORM 1 JAN 73 1473 EDITION OF 1 NOV 65 IS OBSOLETE
S/N 0102-014-6601

SECURITY CLASSIFICATION OF THIS PAGE (When Data Entered)

20. ABSTRACT (Continued)

of the radial profile of ion emission which enhances the net ion current transmitted through the interior of the hollow cathode shank.

CONTENTS

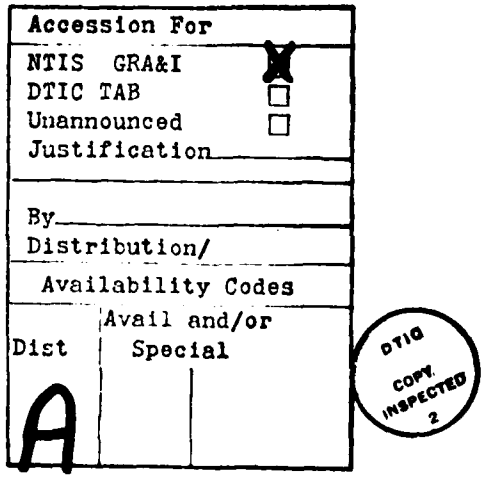

THE USE OF FINITE J_θ FOR INCREASING THE ION EFFICIENCY OF HIGH IMPEDANCE DIODES

I. INTRODUCTION

The efficient generation of intense beams of energetic light ions is a central objective of the NRL Light Ion Fusion Research Program.[1] Over the past several years, focused ion current densities of over 100 kA/cm^2 from terrawatt-level beams have been achieved with magnetically insulated radial diodes at Sandia National Laboratories[2] as well as with pinch-reflex axial diodes at the Naval Research Laboratory.[3] Using diodes of below 2 ohm impedance, ion beam efficiencies of over 70% were achieved in both of the above configurations[4,5] (i.e., — over 70% of the power travelling through the diodes was carried by the light ions generated therein). The question of ion efficiency is critical to the goal of a practical light ion driven inertial confinement fusion (ICF) reactor. As much as possible of a given pulsed power generator's energy must be imparted to the ion beam exiting the diode in order to minimize the number of beam sources necessary for successful pellet ignition as well as to maximize the overall reactor efficiency. These efficiency considerations are well met by the low impedance diodes.

Unfortunately, the high current densities of the ion beams produced by low impedance diodes are not compatible with the focusing and transport systems presently under study for bringing the beams to bear on the proposed fusion targets.[6] In addition, there are strong arguments in favor of the use of high impedance generators in present reactor scenarios.[7] High impedance diodes must be matched to such generators to ensure efficient power transmission but these diodes are plagued by relatively low ion production efficiencies. These low efficiencies are a direct consequence of established diode theory. It has been found semiempirically[8] that the total current flowing through a pinched-beam diode may be approximated by

Manuscript submitted January 28, 1982.

$$I = I_e + I_i \approx 9(\gamma^2 - 1)^{1/2} \frac{R}{D} \left[1 + \left(\frac{eV}{2m_i c^2}\right)^{1/2} \frac{R}{D}\right] \quad (1)$$

where $\gamma = 1 + \frac{V(\text{in } MV)}{0.511}$, R = cathode radius, D = axial anode-cathode ($A-K$) gap, V = diode voltage, and m_i = ion (proton) mass. Implicit in this formula is an ion-to-electron current ratio given by

$$\frac{I_i}{I_e} \geq 0.5 \frac{v_i}{c} \frac{R}{D} \quad (2)$$

where v_i is the mean ion velocity.[9] Thus, for a fixed voltage, increasing the diode impedance translates to decreasing the aspect ratio, R/D. That, in turn, results in a decrease of the current ratio I_i/I_e and a lowering of the ion production efficiency, $I_i/(I_e + I_i)$. This is the crux of the problem addressed by this research. Stated in other terms, Eq. (2) expresses the inverse dependence of the specie current ratio on the ratio of respective species lifetimes in the $A-K$ gap. By increasing the relative electron lifetime over the standard parapotential flow model[10,11] through some modification of the diode field structures, one can hope to significantly beat the R/D limit. The modification studied herein involves the introduction of finite azimuthal current flow in the cathode shank which gives rise to strong tangential magnetic fields along the electron-emitting shank surface. For the J_θ values tested, this technique produced positive results in increasing the effective ion efficiency, η_i, of a 4Ω diode. The same J_θ values tested in a 25Ω diode did not substantially effect its η_i but did modify the density profile of the resultant ion beam. The rationale underlying the finite J_θ techniques as well as the results of the cases tested are presented below.

II. THEORY AND NUMERICAL IMPLEMENTATION

The theories quoted in the previous section assume a predominantly radial flow of electrons cascading from the cathode face at radius, R, down toward the center of the anode. For diode potentials in excess of 1 MV, electrons are quickly accelerated to very near the speed of light, c. Their gap lifetimes, τ_e, are thus on the order of R/c. On the other hand, due to their much greater mass, protons experience little deflection from an axial trajectory across the $A-K$ gap of width, D. They have life-

times, τ_i, of about $D/\bar{v}_i$ where $\bar{v}_i$ is the average ion velocity. Allowing for oscillations in the electron flow yields a pessimistic electron-to-ion τ ratio equal to the current ratio of Eq. (2). In order to increase this ratio, a thin hydrogen-rich foil may be substituted in place of a solid anode. The thickness of the foil is such as to allow an electron to pass through it without excessive energy loss. Behind the foil, a virtual cathode and/or a strong B_θ acts to reflect the electrons back into the $A-K$ gap.[12,13] In such a case, τ_e increases with N, the number of reflections through the foil experienced by a typical electron. That is the essence of the pinch reflex diode (PRD) (see Figure 1) pioneered by NRL. Alternately, the entire diode may be reconfigured from an axial to a radial $A-K$ gap geometry as in Figure 2. In such a diode a combination of imposed B_z and self-generated B_θ magnetic fields constrain electron flow to form an azimuthally symmetric negative space-charge cloud stretching some distance from the cathode into the radial gap. Given the proper choice of operating voltage and other parameters, few electrons will reach the anode ($\tau_e \rightarrow \infty$) and virtually all of the current in this "radial diode" will be carried by the ions in their near-radial trajectories across the gap.[14,15]

With reference to the previously mentioned problem of low ion production efficiency in high impedance diodes, it was reasoned that a possible solution might be to combine the τ_e enhancement created by the electron reflexing anode foil with that arising from the electron flow constraints imposed by the magnetic fields such as those found in a radial diode. Specifically, the standard axial pinch-reflex geometry of Figure 1 might be retained while imposing an azimuthal current density, J_θ, in the tip of the cathode shank.[16] Experimentally, this could be achieved by cutting an azimuthally symmetric pattern of spiral gaps into the shank tip.[17] Increasing the pitch and/or the density of the spirals would increase the effective I_θ component of the net cathode current. This I_θ would give rise to a strong B_r along the intense electron emission region at the tip of the cathode which field would impart a finite angular momentum to those electrons. Several consequences can be expected. First of all, depending upon the strength of $(B_r)_{CATHODE}$, net electron emission along the cathode tip will be reduced due to tangential magnetic field effects (longer electron space-charge retention near the emitting surface).[18] If the impedance remains fixed, this would demand an increase in the ion efficiency. Secondly, finite

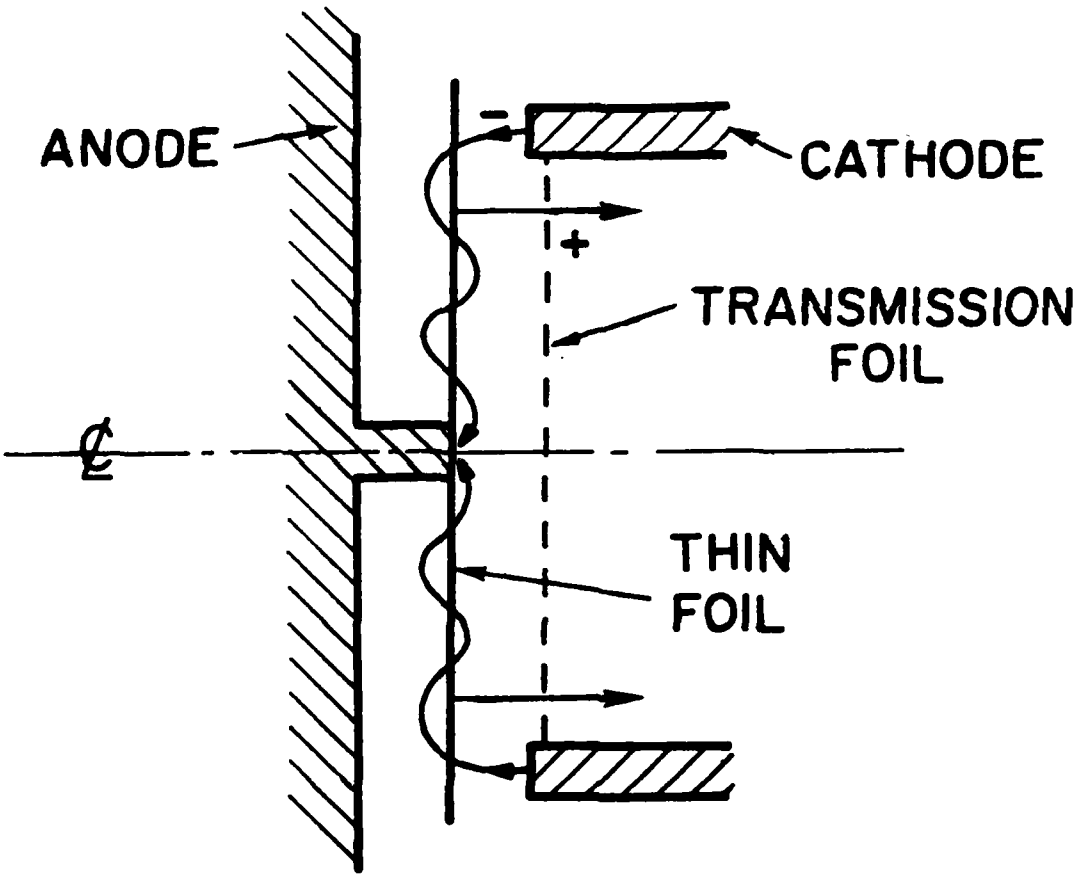

Fig. 1 — The pinch-reflex diode

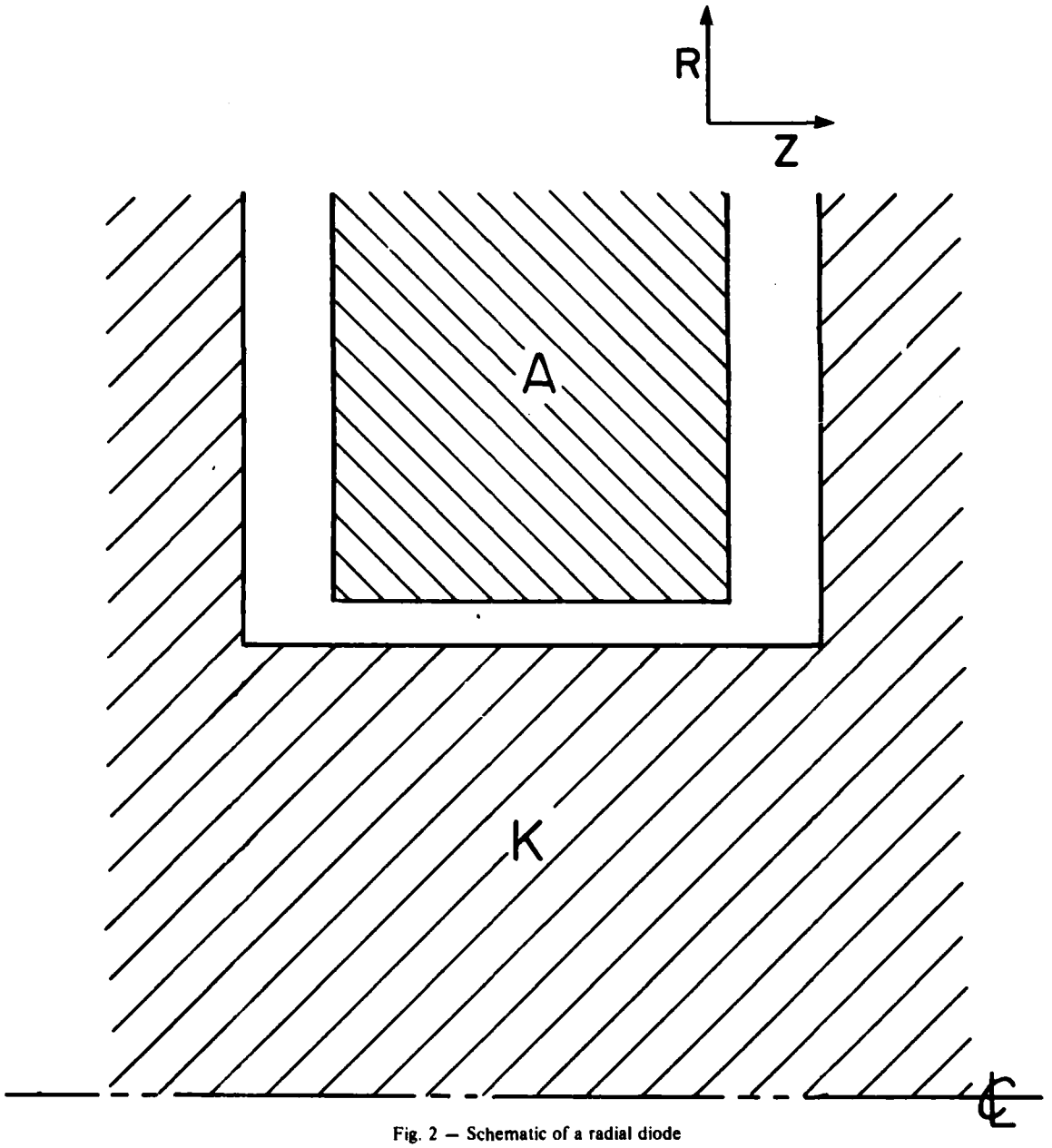

Fig. 2 — Schematic of a radial diode

angular momentum will prohibit electrons from reaching $R = 0$ and thus will inhibit the formation of large electron space-charge accumulations along the diode's central axis. (Such a charge build-up is common in pinch-reflex diodes).[19] This should depress the ion emission peak at the center of the anode and likewise limit the growth of the anode plasma "pimple" at zero radius,[20] thus lowering the average divergence of the ion beam. Thirdly, the additional degree of freedom in the electron motion necessarily complicates the particle's trajectory through the $A-K$ gap. Convoluted figure-eight electron orbits have been observed to increase τ_e in conventional PRD's;[21] the effect should be much more pronounced here. Finally, there is a possibility of noticable magnetic insulation of the electron flow near the anode plasma surface due a combination of electron diamagnetic effects and foil flux exclusion. The resultant formation of an electron charge layer near the ion-emitting surface is a key mechanism for efficient ion production in radial diodes.[22] There are thus four reasons for optimism over this proposed modification for high impedance axial diode design.

NRL's DIODE2D computer code was employed to numerically simulate the steady-state operating conditions for such a J_n-diode (JTD) for various sets of parameters. The details of the code may be found elsewhere.[23] It is sufficient here to point out that DIODE2D calculates equilibrium electric and magnetic field strengths over an $NZ \times NR$ mesh of discrete data points on a pre-determined computational region corresponding to an arbitrary $R-Z$ planar cross-section passing through the diode's centerline. Complete azimuthal symmetry is assumed. A finite number of macro-electrons and macro-protons having correct, physical charge-to-mass ratios are advanced timestep-by-timestep across the mesh in a relativistically covariant manner. A steady-state solution is sought both for field structures as well as for particle flows. No time-dependent phenomena are actually treated.

The dimensions of the diode numerically modeled here come from actual experimental apparatus designed by NRL personnel for light ion beam research on the AURORA and PBFA-I pulsed power generators. At the U.S. Army's Harry Diamond Laboratories (HDL), one of the four 50-ohm lines of the AURORA machine was fitted with a custom designed PRD.[24] The experimental arrangement is depicted in Figure 3. Details of the diode structure at the tip of the device are shown in Figure 4. All

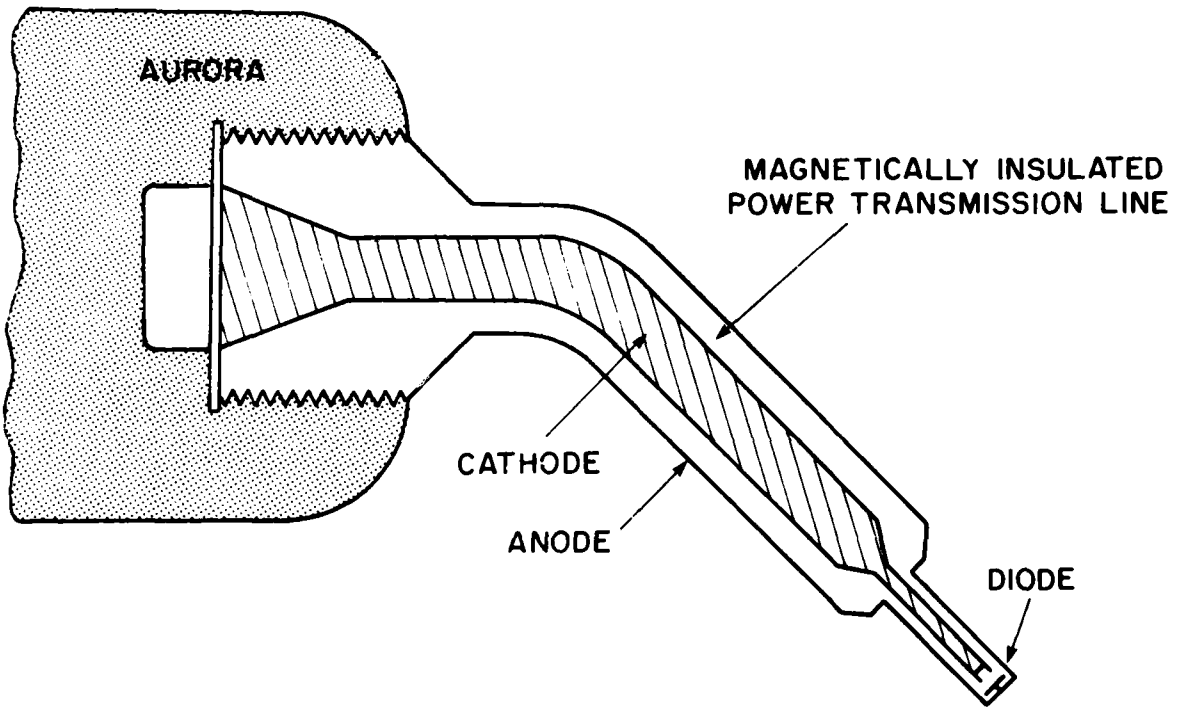

Fig. 3 — The NRL-AURORA ion diode experiment

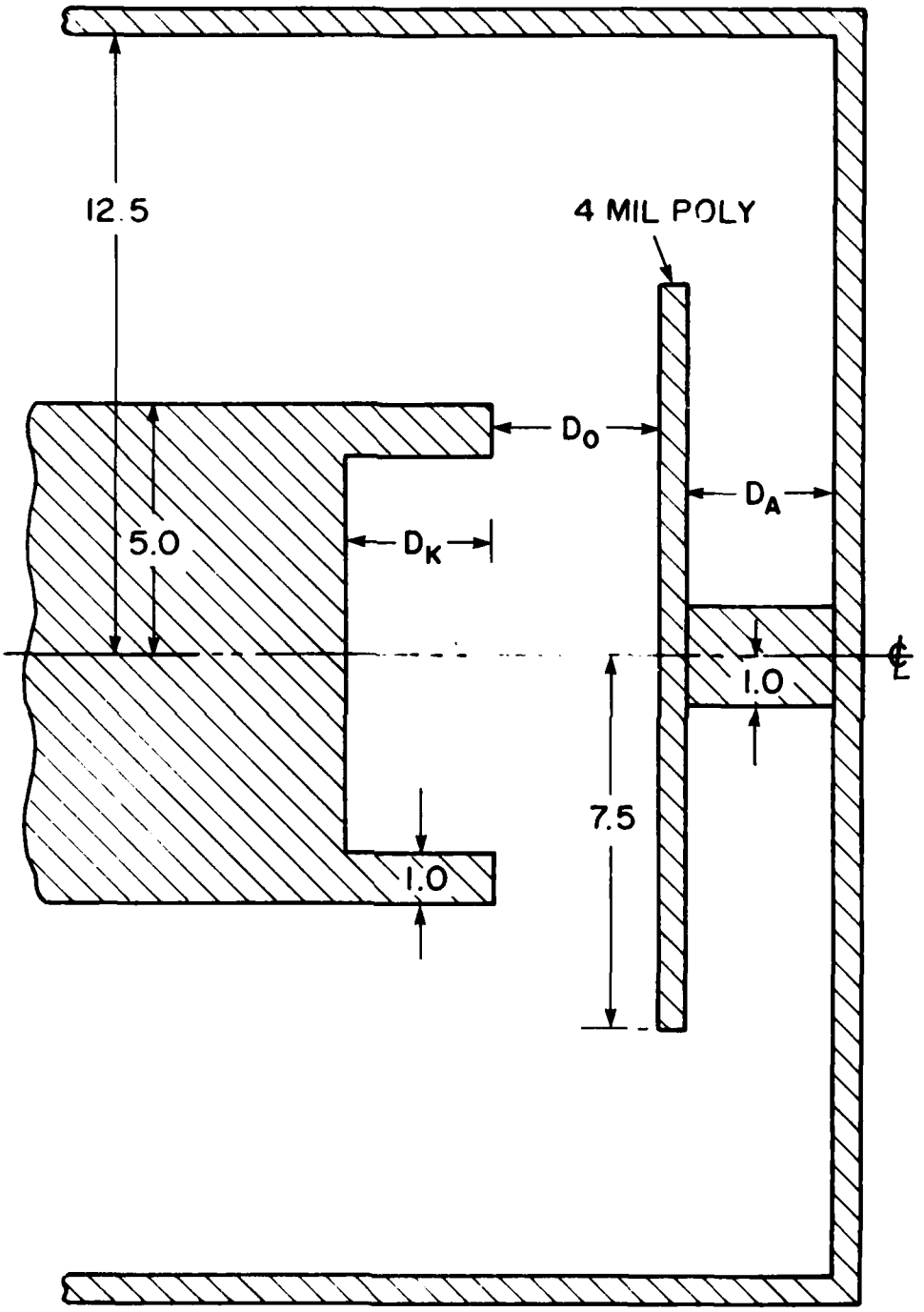

Fig. 4 — The diode to be modeled

radial dimensions are given in centimeters. Of the three, variable axial dimensions indicated, the most significant is D_0, the anode-cathode ($A-K$) gap. For a fixed cathode radius of five centimeters, the value of D_0 essentially determines the diode impedance and efficiency for a given applied voltage via Eqs. (1) and (2). It may be further noted that the diode of Figure 4 is in a "negative polarity" configuration corresponding to the early experimental runs on AURORA. The cathode is the central conductor of the coaxial line and the resultant ion beam is accelerated toward the machine, making beam diagnostics very difficult and beam transport impossible. In more recent experiments, the central conductor was switched to positive polarity[25] and the anode foil and cathode appropriately reversed. Such a change in polarity can be expected to significantly modify the source-free electric field structure only at large radii and probably have little impact on the dynamics of particle flows in the active $A-K$ gap below five centimeters radius. This relative isolation of the active particle flow region from the large radius field structure similarly encouraged the use of the same diode structure of Figure 4 to model the 4-6 ohm PRD being designed by NRL for use on the individual lines of PBFA-I at Sandia Labs. Only the diode voltage and axial dimensions were changed. Specifically, the AURORA simulations were conducted with $D_0 = 3.3$ cm at 5.0 MV while those for PBFA-I were with $D_0 = 0.66$ cm at 2.0 MV.

The volume that must be simulated using the DIODE 2D code extends radially from the central axis to the inner radius of the anode shell and axially from the plane corresponding to the recessed foil face of the cathode out to the inner plane surface of the vacuum vessel, anode shell. Since it presumes azimuthal symmetry, the computer code only deals with a single $R-Z$ planar cross-section extending out from the centerline. This computational region is presented in Figure 5. The grid points are shown as dots and correspond to the center of their respective rectangular data cells. Given the monolayer of guard cells completely surrounding the entire region in which particles are "allowed," a total of $(NZ + 2) \times (NR + 2) = 66 \times 52 = 3{,}432$ mesh points are used. The bottom boundary corresponds to the central axis ($R = 0$) of the diode. The right and upper boundaries represent the anode shell and are maintained at the full anode potential. The left boundary is kept at zero voltage up to cell 22 and

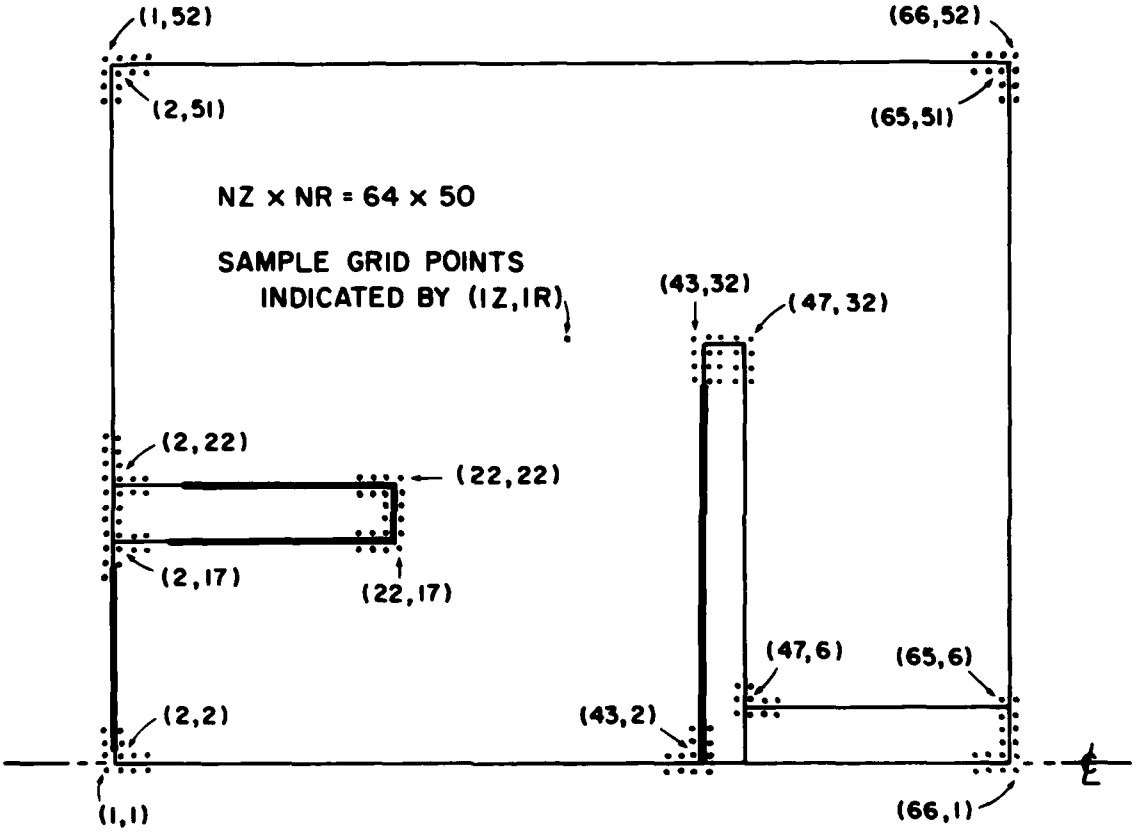

Fig. 5 — Set-up of the numerical simulation region

then increased logarithmically up to the anode voltage. Perfectly conducting cathode and anode surfaces are included in the computational region as shown in Figure 5. They are treated numerically via a capacitance matrix technique described elsewhere (see Ref. 26). On the order of 10^4 macroelectrons and 10^4 macroprotons participate in the simulation at steady state. These macroparticles are emitted at their respective electrodes along the heavy-lined surfaces. Axial currents in the cathode shank and in the anode stalk are treated rigorously as a function of z in order to ensure an accurate distribution of B_θ throughout the diode. The results of these numerical simulations as well as a summary of the conclusions which could be drawn from them are presented in the following two sections.

III. RESULTS

1. AURORA

The first diode modeled was one appropriate for use on the AURORA machine. The diode voltage was fixed at 5 MV. The axial spacing between grid points was set to $\Delta Z = 0.15$ cm, yielding an $A-K$ gap, D_0, of 3.3 cm (see Figure 4). For a cathode radius of 5.0 cm, Eq. (1) predicts a diode current of 156.7 kA yielding an impedance of 32 ohms. Equation (2) predicts an ion efficiency, η_i, of only 0.0725 $\left[= \dfrac{I_i}{I_e + I_i}\right]$. These predictions fall far short of observed results. A diode with the above geometry and voltage was tested experimentally and computationally by NRL and the results were just recently published.[27] The numerical simulation quoted in that paper found a steady-state diode current of 205 kA of which 40 kA were carried by protons. This amounts to a diode impedance of 24 ohms and an ion efficiency, η_i, of about 0.195. The average experimental results reported in the same paper were $I_{\text{diode}} \approx 250$ kA (20 ohms) and $\eta_i \approx 0.20$. It should be noted that the experiment started with an $A-K$ gap of 4.9 cm but that gap closure due to electrode plasma expansion was expected to have narrowed that to about 3.3 cm by the time of peak current in the power pulse. Those findings clearly contradict Eqs. (1) and (2). High impedance operation gives rise to new diode phenomena not properly treated in that earlier analysis. The need for a more complete theoretical treatment still exists. Until one is found, numerical simulation is the best nonexperimental tool available for analysis.

As an additional "benchmark" for the results to be reported here, a numerical simulation was carried out on the same diode but in positive polarity. The results were: I_e = 182 kA, I_i = 56 kA, I_{diode} = 238 kA, Z = 21 ohms, and η_i = 0.235. This is in agreement with the negative polarity experiment indicating that changes in the electric field configuration along the far boundaries of the diode have little effect on the physics of the $A-K$ gap. Higher currents were achieved here than in the negative polarity simulation probably because no electron emission along the cathode shank had been permitted in that earlier run. The electron particle plot of Figure 6 shows very significant electron flow from the shank. To test the effects of J_θ in the shank, a negative polarity was again assumed in the diode to conform to the quoted experiments.

The azimuthal current was imposed in the cathode shank in a very straightforward manner. Referring back to Figure 5, a constant, predetermined value of J_θ was assumed in each of the data cells in the rectangular region stretching from IZ = 6 through IZ = 21 and from IR = 18 through IR = 21 (i.e., —a cross-sectional area of 2.4 cm^2). As a first test for the idea, a value of J_θ = 1 kA/cm^2 was arbitrarily chosen giving 2.4 kA of azimuthal current flowing through the shank. The effect of this small I_θ was quite pronounced. In a simulation of electron-only flow, a net current of 209 kA was achieved (diode impedance of 24 ohms). A sampling of electron positions in the steady state for that case is presented in Figure 7. The shaping of the electron flow by the shank's B-field is clearly discernable. Notice, in particular the intense stream of electrons from the top rear of the shank arcing up and across the gap along the field lines. There also seem to be electrons that are emitted from the inside shank surface and then flung upward behind the foil. The net effect is an increase in the mean radius of electron impact on the anode foil. Thereafter in the simulation, proton emission was turned on along the entire front face of the anode foil. The new equilibrium with both species present yielded the following: I_e = 244 kA, I_i = 41 kA, I_{net} = 285 kA, Z = 17.5 ohms, and η_i = 0.144. Thus, the ion production efficiency decreased by 0.091 or almost 40% while the impedance dropped by about 17% compared to the J_θ = 0, "benchmark" case. This was unexpected but an examination of the sample particle plots of Figure 8 suggests two causes. First of all, the electron stream is illuminating only a

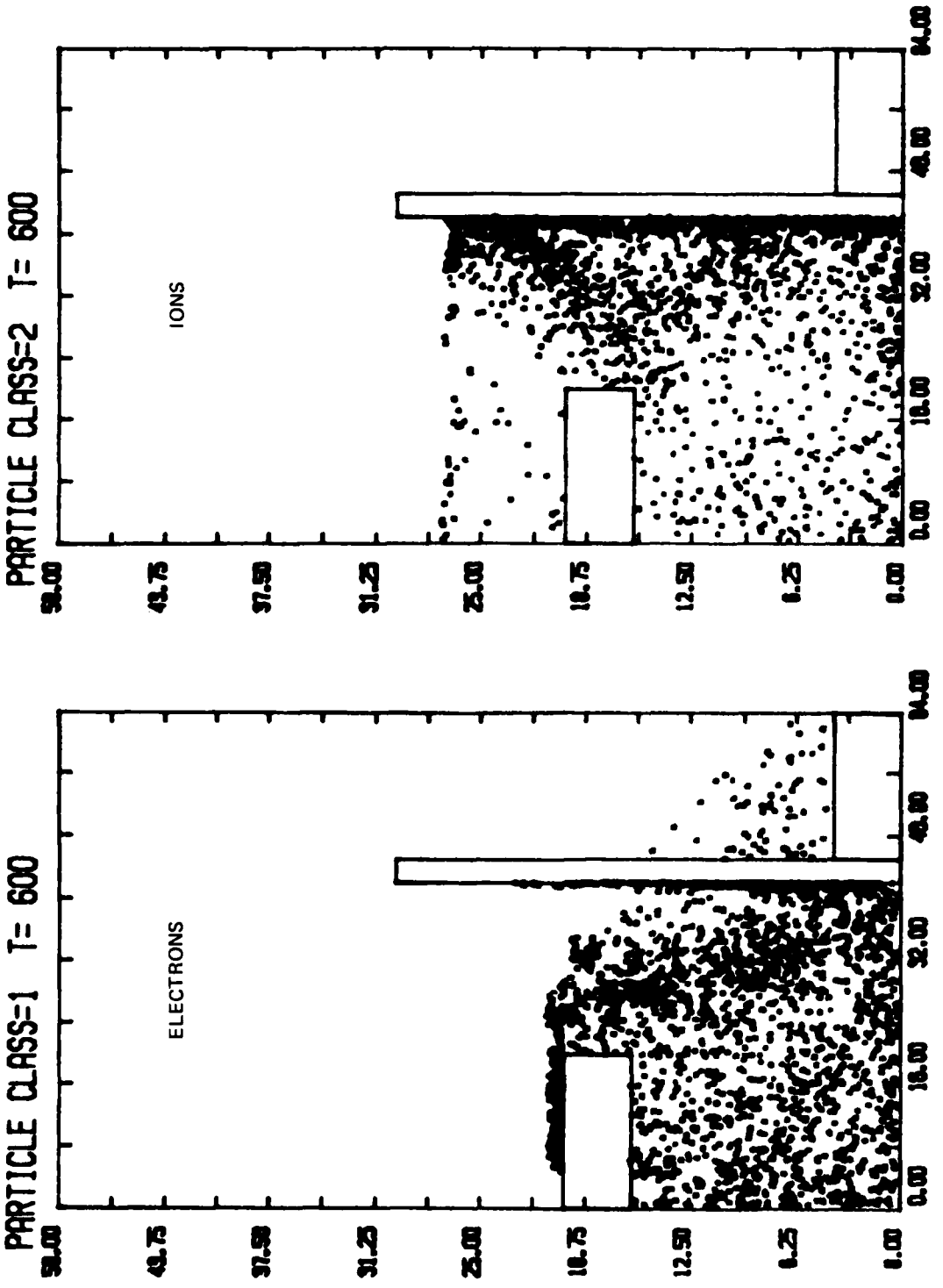

Fig. 6 — AURORA electron and ion flow for $J_\mu = 0$.

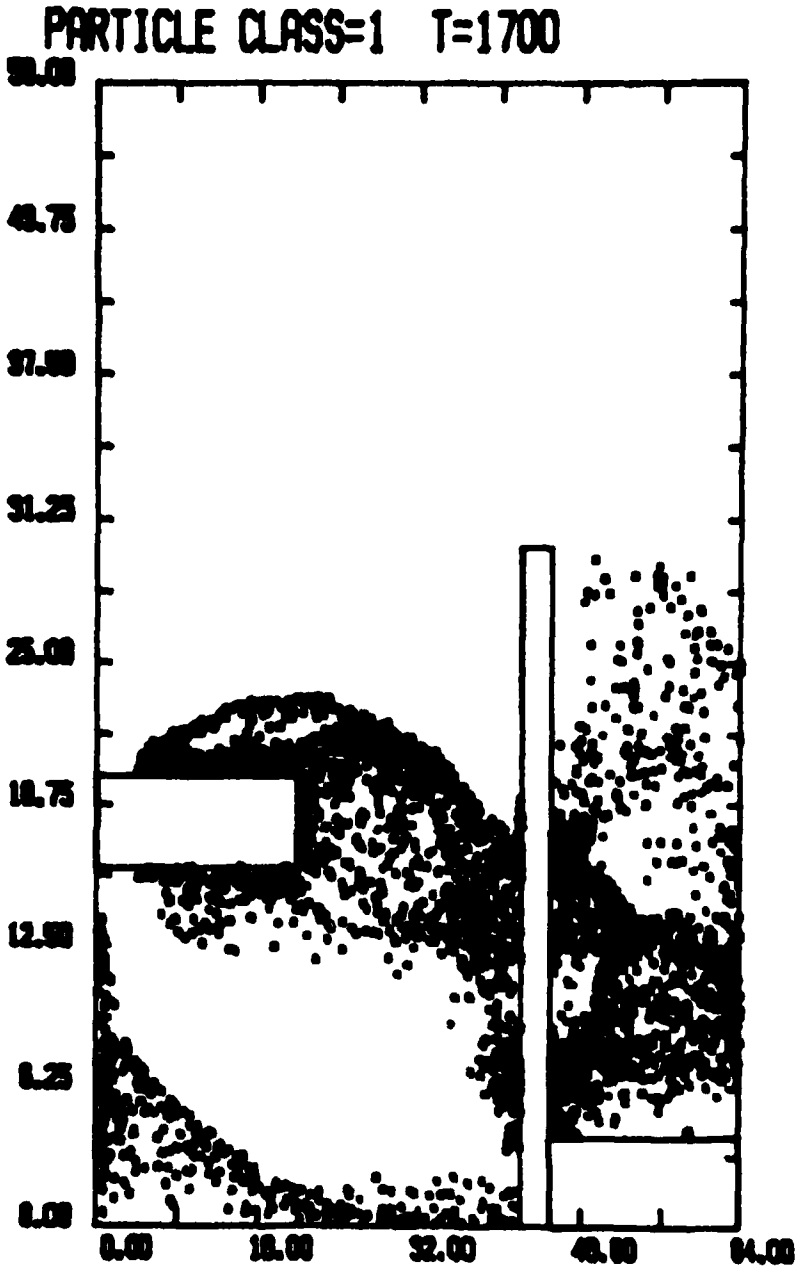

Fig. 7 — AURORA electrons-only flow for J_e = 1 kA/cm^2

relatively small area of the anode. This is lowering η_i. Secondly, the shank magnetic field is still enhancing the net shank electron emission by keeping large numbers of electrons emitted in the rear of the shank from hitting the forward portions of the shank and lowering emission there as is normally the case. This "layering" of the shank electron flow can be seen in Figure 8.

In order to remedy this situation, a better choice for J_θ was sought. The simulation code was reset to the electrons only equilibrium and J_θ was set to 10 kA/cm^2 or a total azimuthal shank current of about 24 kA. The results can be seen in Figure 9. This case was not run to equilibrium. The net effects were in a beneficial direction albeit to an extreme. The mean radius of electron impact on the anode foil was indeed increased. In addition, although emission on the outer surface of the shank was again enhanced, emission on both the inner surface as well as along the cathode tip was greatly curtailed due to direct magnetic insulation. The net electron current fell to about 60 kA.

As a reasonable intermediate choice J_θ was taken as 4 kA/cm^2 yielding I_θ = 4.8 kA. This case was run and again both the impedance and the efficiency dropped. Specifically, the observed steady-state currents were I_e = 257 kA, I_i = 34 kA, and I_{diode} = 291 kA giving an impedance of 17.2 ohms and an ion efficiency of 0.117. As shown in Figure 10, the cause of the problem seems to be very similar to that for the J_θ = 1 kA/cm^2 case. Once again although the shank B-field is reducing emission at the shank tip, it is also preventing much of the normal self-suppression of electron emission over the bulk of the outer shank surface. One improvement is the larger average radius of electron impact on the anode foil. This confirms the ability of the shank J_θ to radially direct the $A-K$ gap electron flow. Still, the anode foil area illuminated by the electrons is rather narrow and most electrons appear to transit immediately to the solid anode surface in the rear without reflexing again through the foil. This tightly restricted nature of the electron flow and resultant ion flow is illustrated by the plots in Figure 11. These radial profiles of ion current density collected at the cathode show distinct regions of enhancement. All three curves show peaks near the central axis due to the strong flow of tightly pinched electrons emitted from the rear cathode foil surface inside the shank. All three likewise have peaks between R = 4 cm and R = 5 cm corresponding to ions collected by the protruding cathode

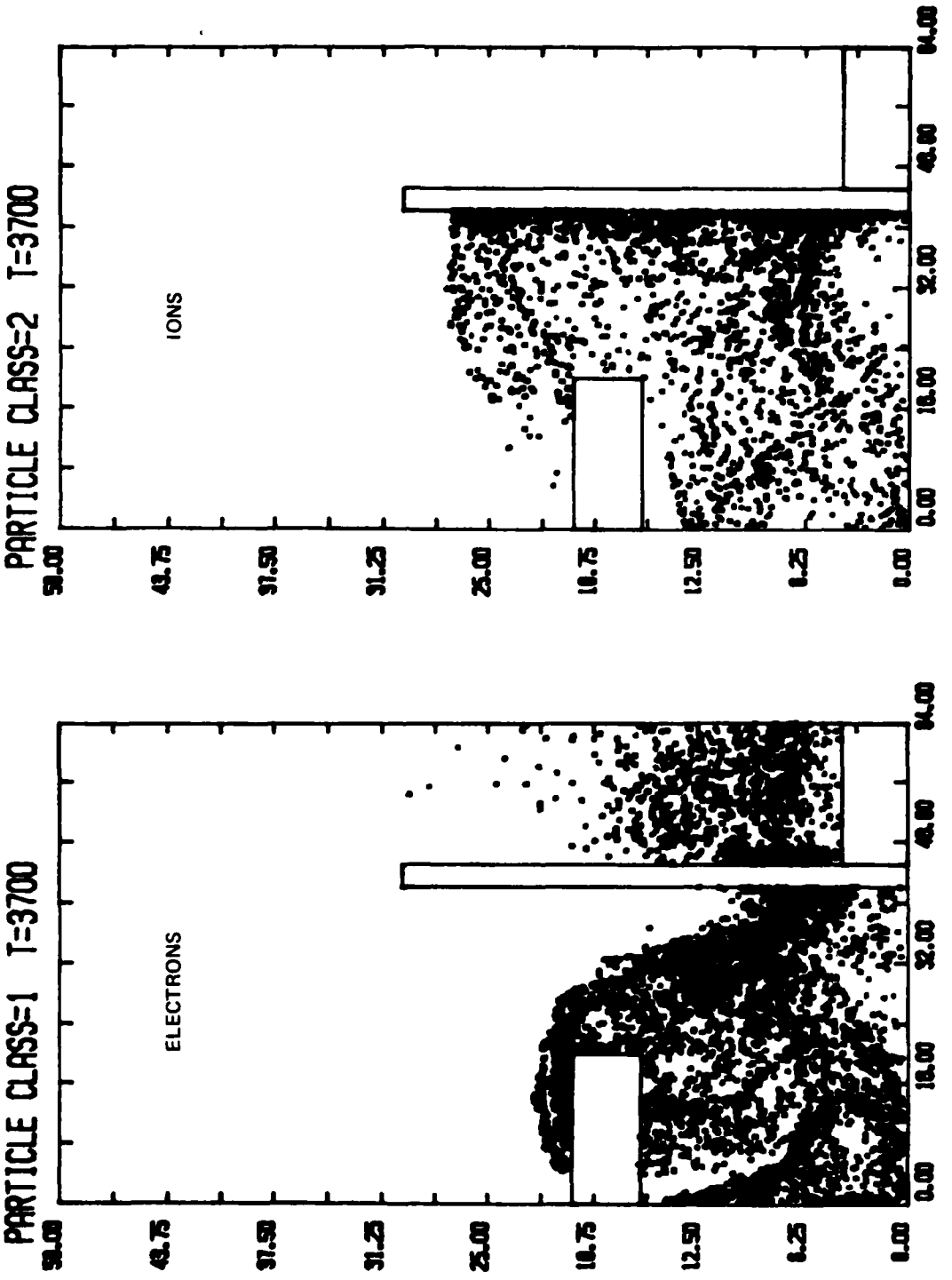

Fig. 8 — AURORA electron and ion flow for $J_0 = 1$ kA/cm^2

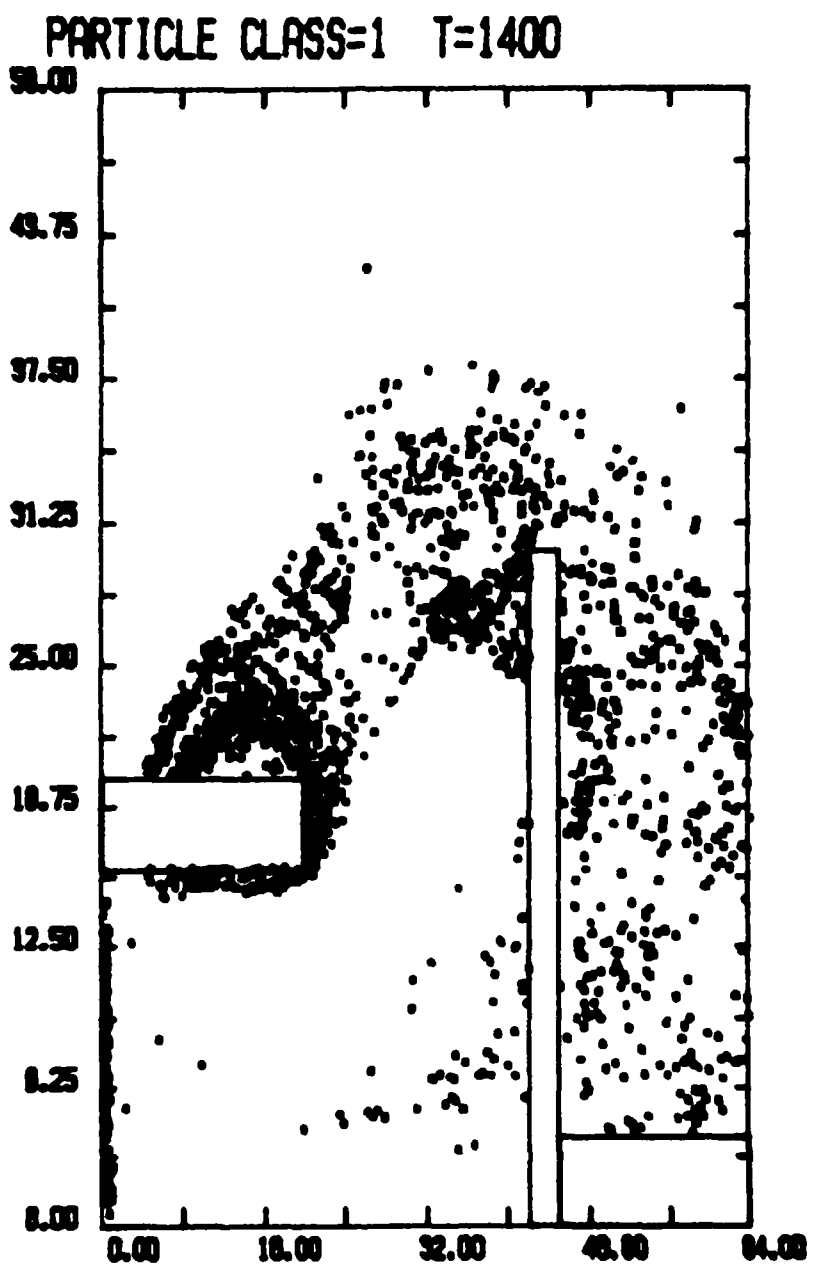

Fig. 9 — AURORA electrons-only flow for J_a = 10 kA/cm^2

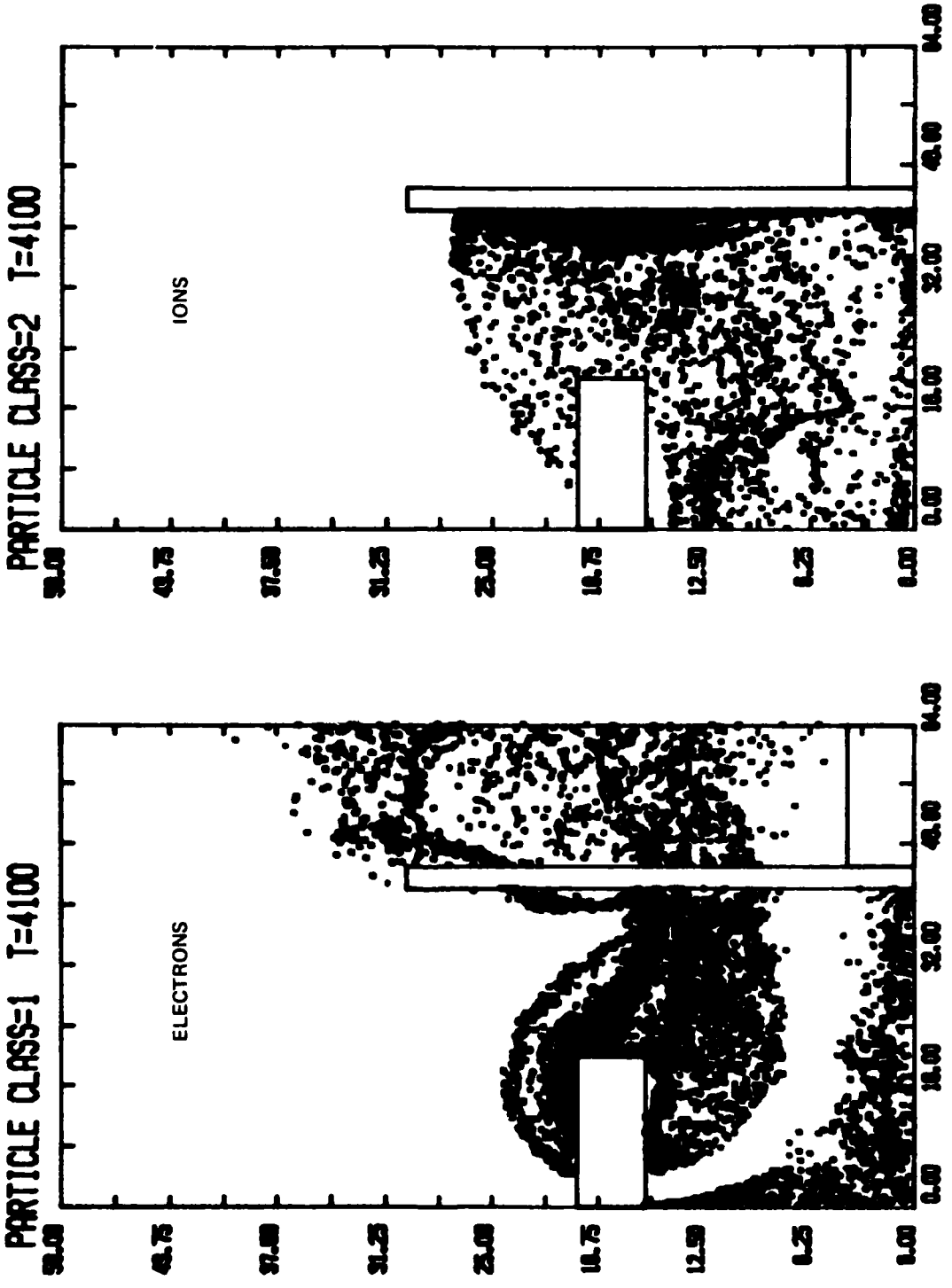

Fig. 10 — AURORA electron and ion flow for $J_0 = 4$ kA/cm^2

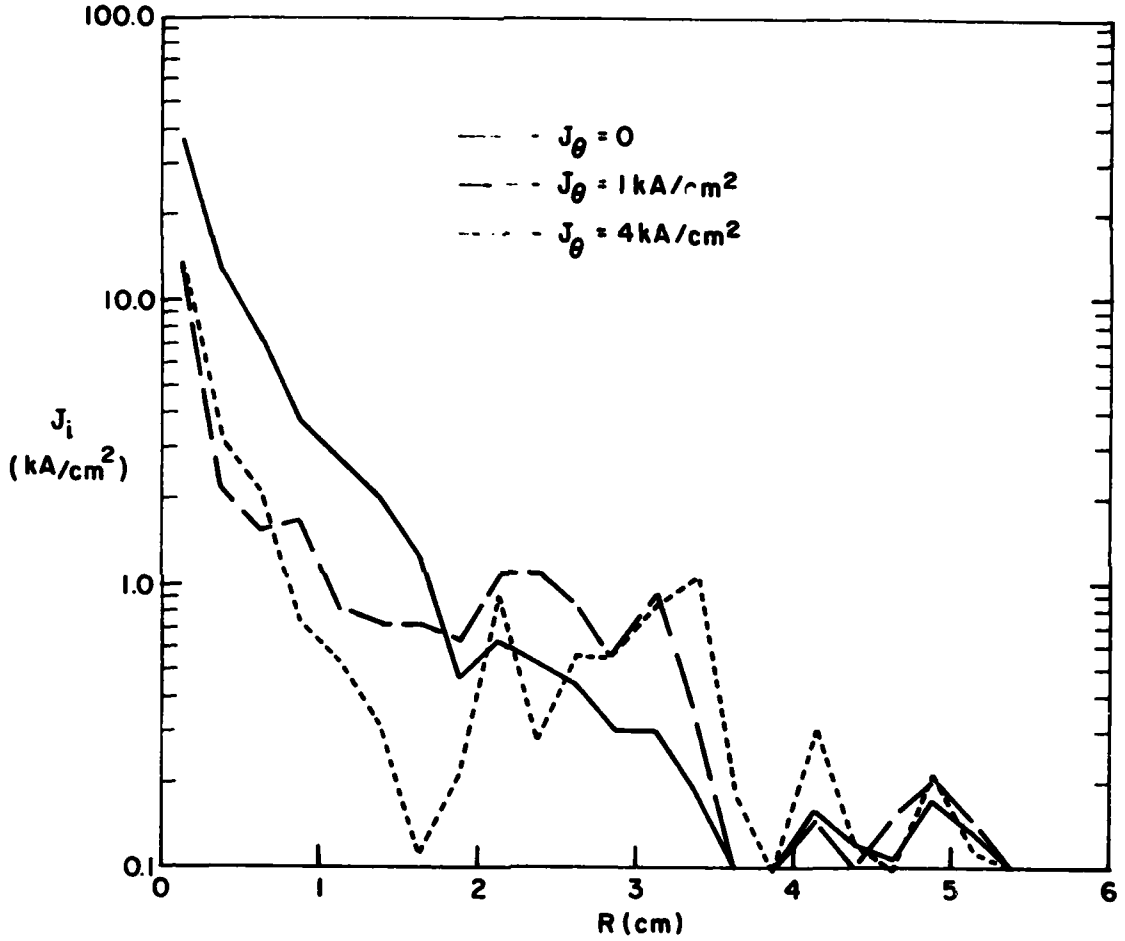

Fig. 11 — Radial profiles of AURORA ion current density collected at cathode

shank. However, in terms of net ion current collected at the various radii, the $J_{\theta} = 4\ kA/cm^2$ profile indicates that most of the ion current is flowing in a hollow cylindrical shell. This capability to shape the ion current density emerging from the diode may prove useful for future applications. Unfortunately it is clear that whatever other benefits $(J_{\theta})_{shank}$ may offer for the AURORA diode, an improvement in ion production efficiency does not appear to be among them.

2. PBFA-I

Much of the on-site experimental effort of the NRL Light Ion Fusion Group has been dedicated to the design of an ion-efficient, 3-5 Ω diode for use on individual modules of the PBFA-I pulse power generator at Sandia National Laboratories. This work has been conducted on the GAMBLE-II machine at NRL.[28] A typical diode configuration used in that research is illustrated in Figure 12. The outer radius of the cathode shank was 3 cm while its thickness varied between 4 and 8 mm. An $A-K$ gap of approximately 5 mm was maintained although electrode plasma expansion gap closure at a normal rate of 3 $cm/\mu sec$ over the 40 ns power pulse probably created an effective $A-K$ gap of 3.8 mm. The effective diode voltage was about 1.8 MV. For these parameters and a gap of 5 mm, Eqs. (1) and (2) predict an impedance of 7.1 ohms and an ion efficiency, η_i, of 0.186. An effective gap of 3.8 mm changes these to 5.1 ohms and $\eta_i = 0.245$ respectively. Experimentally, the diode ran at from 3 to 5 ohms and achieved 0.25 to 0.35 ion efficiencies in 40% of the shots (see Figure 13). The theoretical predictions using $D_0 = 3.8$ mm were quite close. Numerical simulations were conducted for a similar 4 ohm diode at 1.8 MV and a η_i of about 0.40 was observed.[29] Therefore, theory, experiment, and numerical simulation all call for between 0.25 and 0.40 ion efficiency.

To numerically test the effects of a shank J_{θ} on diode performance in this lower impedance regime of 3-5 ohms, the same model diode as that used for the AURORA simulations (see Figure 4) was employed except that the voltage was lowered to 2 MV and D_A, D_0, and D_4 were set equal to 0.60., 0.66, and 0.57 cm respectively. For those parameters, theory predicts 4.9-ohm operation and an η_i of at least 0.247. The experimental and numerical results from the actual GAMBLE-II diode would

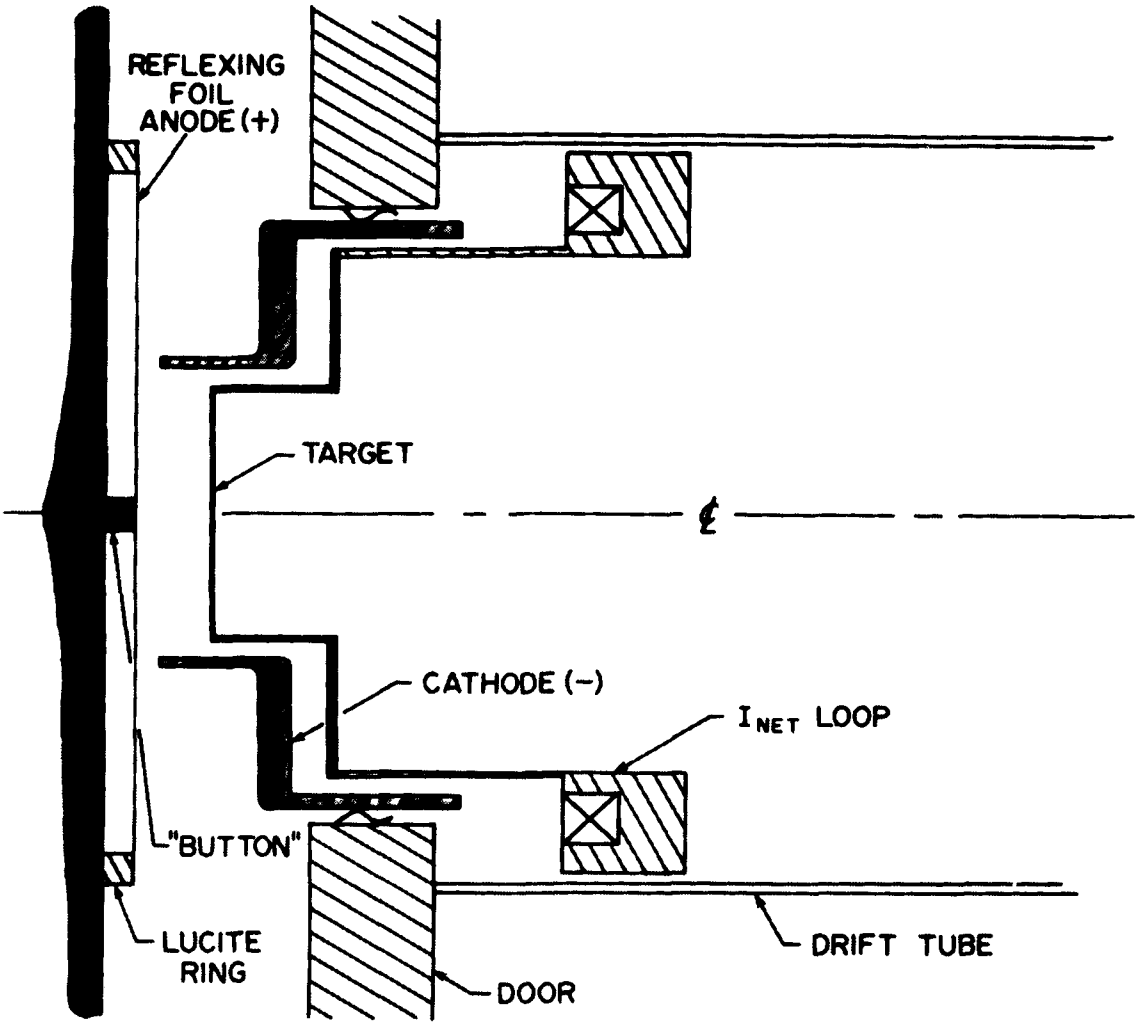

Fig. 12 — The high impedance Gamble II Test Diode for PBFA-I (courtesy of G.J. Stefanakis and D. Mosher).

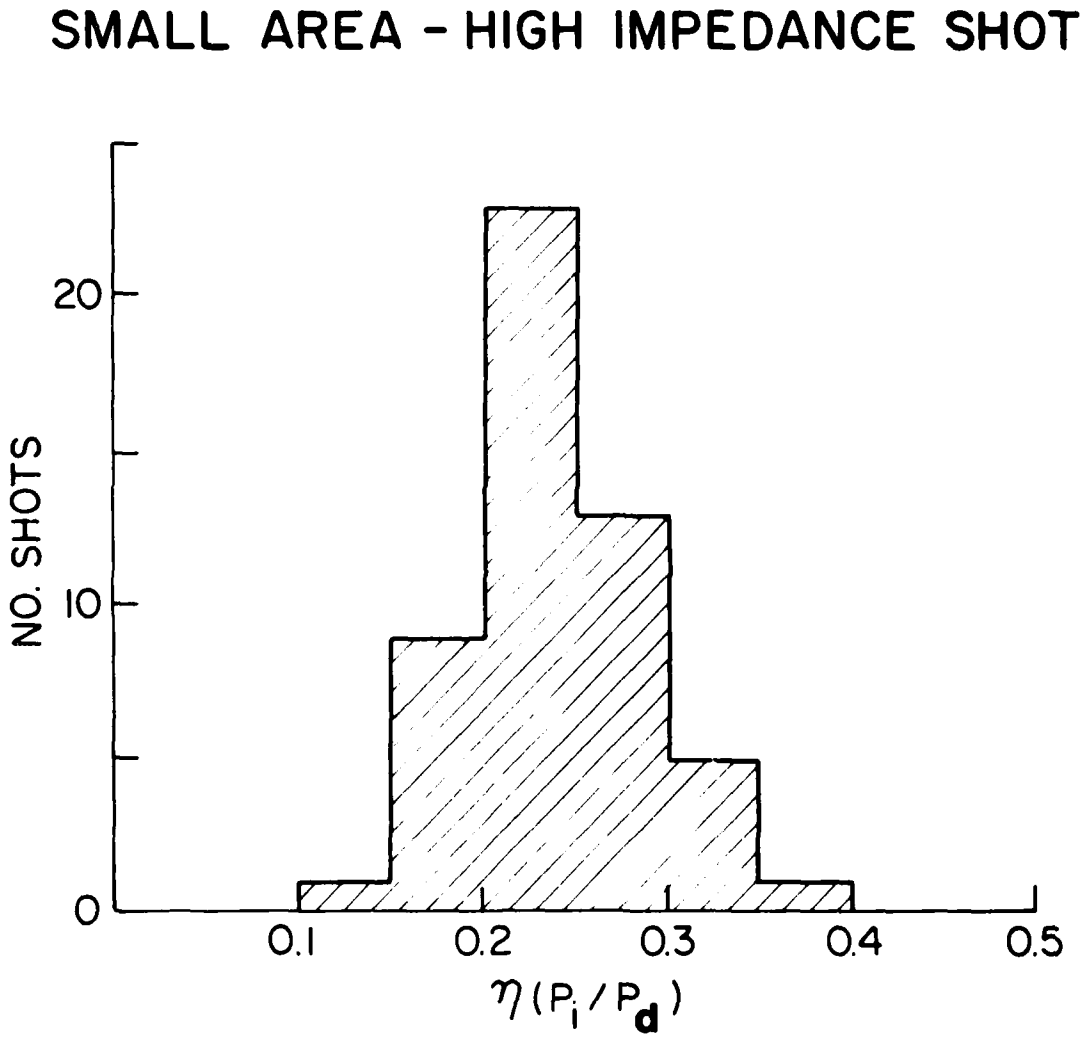

Fig. 13 — Statistical distribution of η, for the 4Ω diode (courtesy of S. J. Stefanakis).

indicate that those predictions are pessimistic. The computational results which follow will use the numerical run cited in the previous paragraph as a $J_{\theta} = 0$ "benchmark."

The total simulation was run in such a way as to sequentially test the following cases: (a) $J_{\theta} = 0$ with only electrons, (b) $J_{\theta} = 2$ kA/cm^2 with only electrons, (c) $J_{\theta} = 2$ kA/cm^2 with ions and electrons, and (d) $J_{\theta} = 4$ kA/cm^2 with ions and electrons. The traces of the electron and ion currents collected by the opposing electrodes during this run are plotted in Figure 14. The near-steady state at $T = 400$ for electron flow in the $J_{\theta} = 0$ case was used as the starting point for the imposed J_{θ} tests. This azimuthal current density was again imposed on the numerical mesh points in the rectangular cathode shank cross-section extending from $IZ = 6$ through $IZ = 21$ and from $IR = 18$ through $IR = 21$. With the new axial grid spacing of $\Delta Z = 0.03$ cm, this amounts to an area of 0.48 cm^2. The first test case, with $J_{\theta} = 2$ kA/cm^2, therefore amounts to a net azimuthal current of 0.96 kA. This shank current component was "turned on" at $T = 400$. At $T = 600$, ion emission was initiated along the front anode surface. The test for this particular value of J_{θ} was terminated at $T = 1200$, well before a steady state had been achieved. The reason for the early termination was the [illegible] development of the electron flow pattern in the diode. This is illustrated by the sequence of sample electron position snapshots shown in Figure 15. The first shot depicts the electrons-only flow for $J_{\theta} = 0$ at $T = 400$. A substantial amount of reflexing through the anode foil is apparent as is a significant loss of electrons directly to the solid anode surface behind the foil. A stream of electrons emitted from the recessed cathode foil inside the shank can also be seen. Note that the electron mainstream initially impacts the anode foil almost exactly opposite the cathode shank face (i.e.-between 4.0 and 5.0 cm in radius). The electrons-only flow with $J_{\theta} = 2$ kA/cm^2 in the second shot of the series embodies the same electron flow characteristics as the $J_{\theta} = 0$ case but with significantly more radial pinching. Few electrons are impacting the anode foil opposite the shank face. In fact, a distinct gap has opened in the flow above a radius of 4.2 cm within a millimeter of the foil surface. Finally, in the last of the three segments of Figure 15, the electron flow is shown at a time when the main ion flow has traveled about halfway toward the recessed cathode foil. Only the anode foil below 3.0 cm in radius is being illuminated by

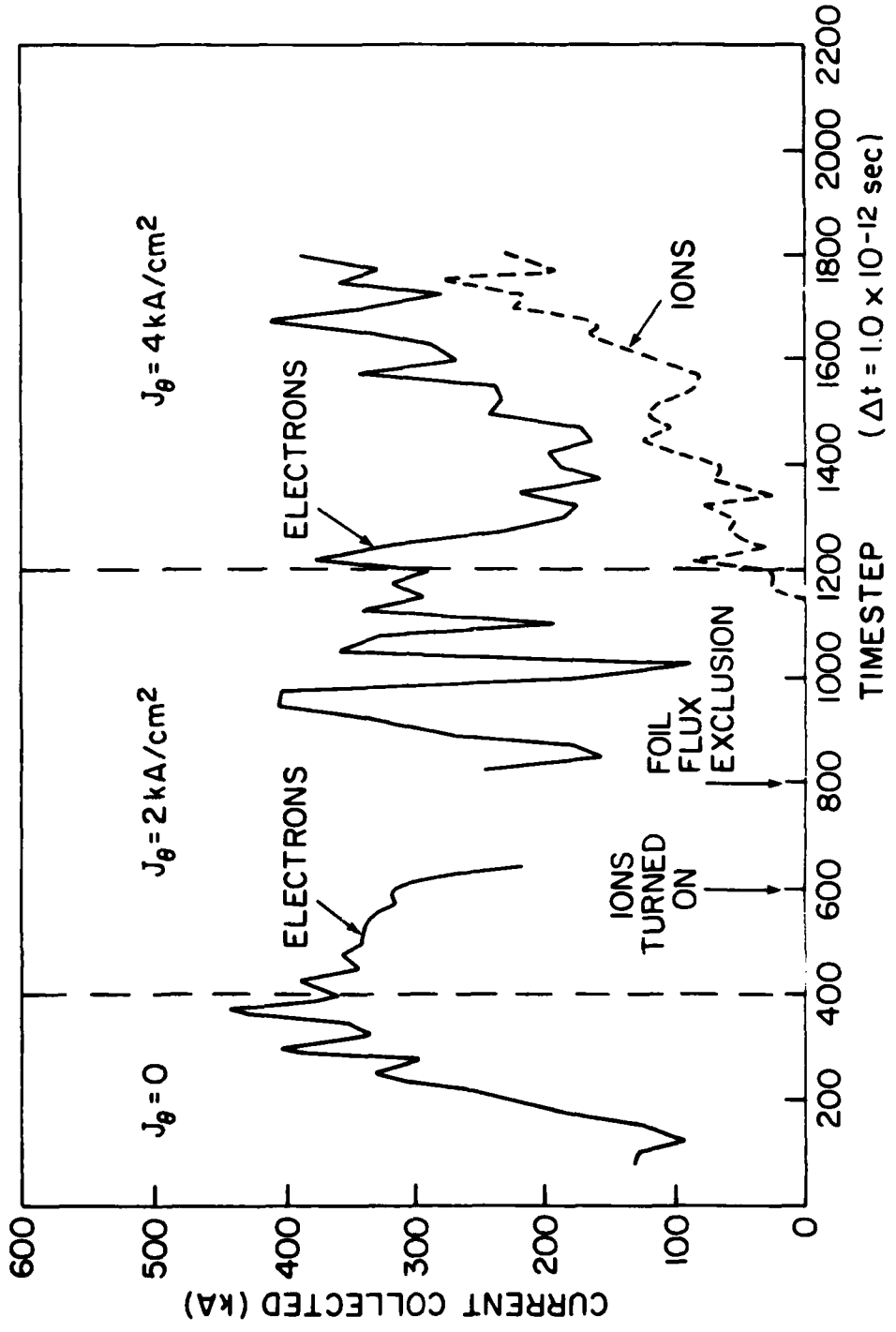

Fig. 14 – Temporal traces of collected electron and ion currents from the PBFA-I diode simulation

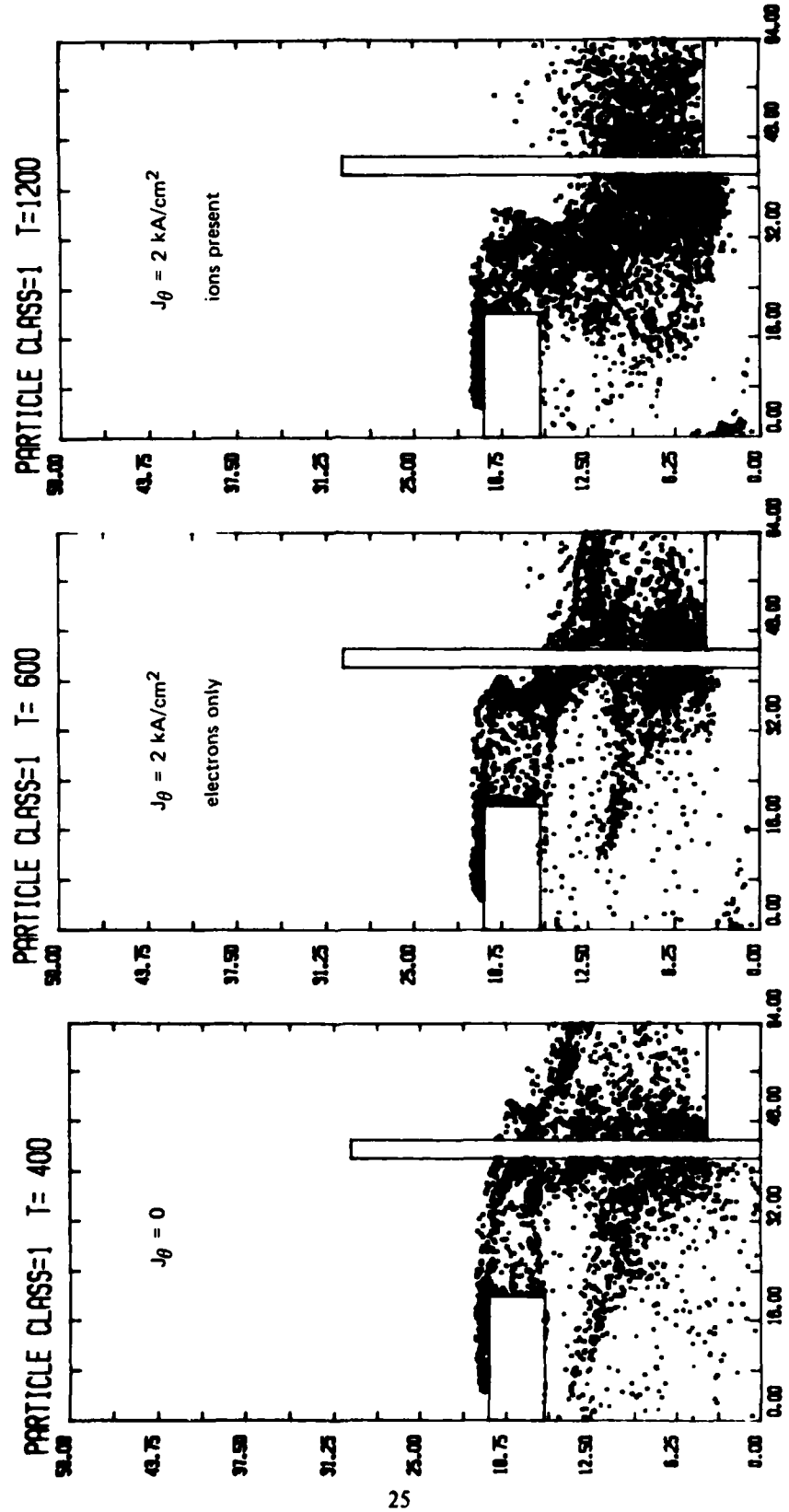

Fig. 15 — Comparison of PBFA-I electron flow patterns

electron impacts. This translates to no enhancement of ion emission over the large anode foil areas at larger radii.

In order to remedy the electron flow pattern problem, the beneficial effects of elevated J_n are recalled (see Figure 9). At $T = 1200$, the azimuthal shank current density was doubled to 4.0 kA/cm^2. When equilibrium was reached at $T = 2600$, the sample electron and ion flow appeared as shown in Figure 16. There is a definite improvement of anode illumination by electrons compared with the J_n = 2 kA/cm^2 case as indicated by Figure 17 which provides radial profiles of accumulated numbers of electron hits (not necessarily absorptions) across the face of the anode foil. The numbers given are relative and may be normalized to the total electron current in each case if so desired. For the purposes of this comparison, take I_e to be the same for each case. The J_n = 4 kA/cm^2 profile yields the most sharply peaked hollow electron beam at the highest mean radius. The sharpness of the profile is not unlike that observed in hollow cathode diodes having strong applied axial magnetic fields.[30] The equilibrium total currents were I_e = 322 kA and I_i = 232 kA yielding an impedance of 3.6 ohms and an ion production efficiency of 0.42 compared to the $J_n = 0$ benchmark of 4.0 ohms and $\eta_i = 0.40$.

The observed gain in net ion efficiency of 0.02 is insignificant, especially when taken in combination with the 0.4 ohm drop in diode impedance. There is a difference, however, between the total ion current flowing in a diode and the net ion current which can be extracted from a diode through the hollow cathode shank. Only the latter is useful from a practical, experimental standpoint. This distinction is crucial in judging the merits of the *J*-theta diode. Plotted in Figure 18 are the radial profiles of ion current density striking the cathode for both the $J_n = 0$ case (a $1/r$ profile with a central plateau corresponding to the location of the anode foil support button) and for the J_n = 4 kA/cm^2 case. For $J_n = 0$, a full 22% of the total ion current is lost to the cathode shank. This reduces the *effective* ratio of useful (extractable) ion current to total diode current to 0.31, in good agreement with the previously mentioned experimental observation of 0.25 to 0.35 ion efficiencies in 40% of the 4Ω shots actually conducted on GAMBLE-II. In comparison, for J_n = 4 kA/cm^2, only 11% of the total ion current is lost to the shank, leaving an *effective* ion efficiency of 0.374. This amounts to an improvement of over

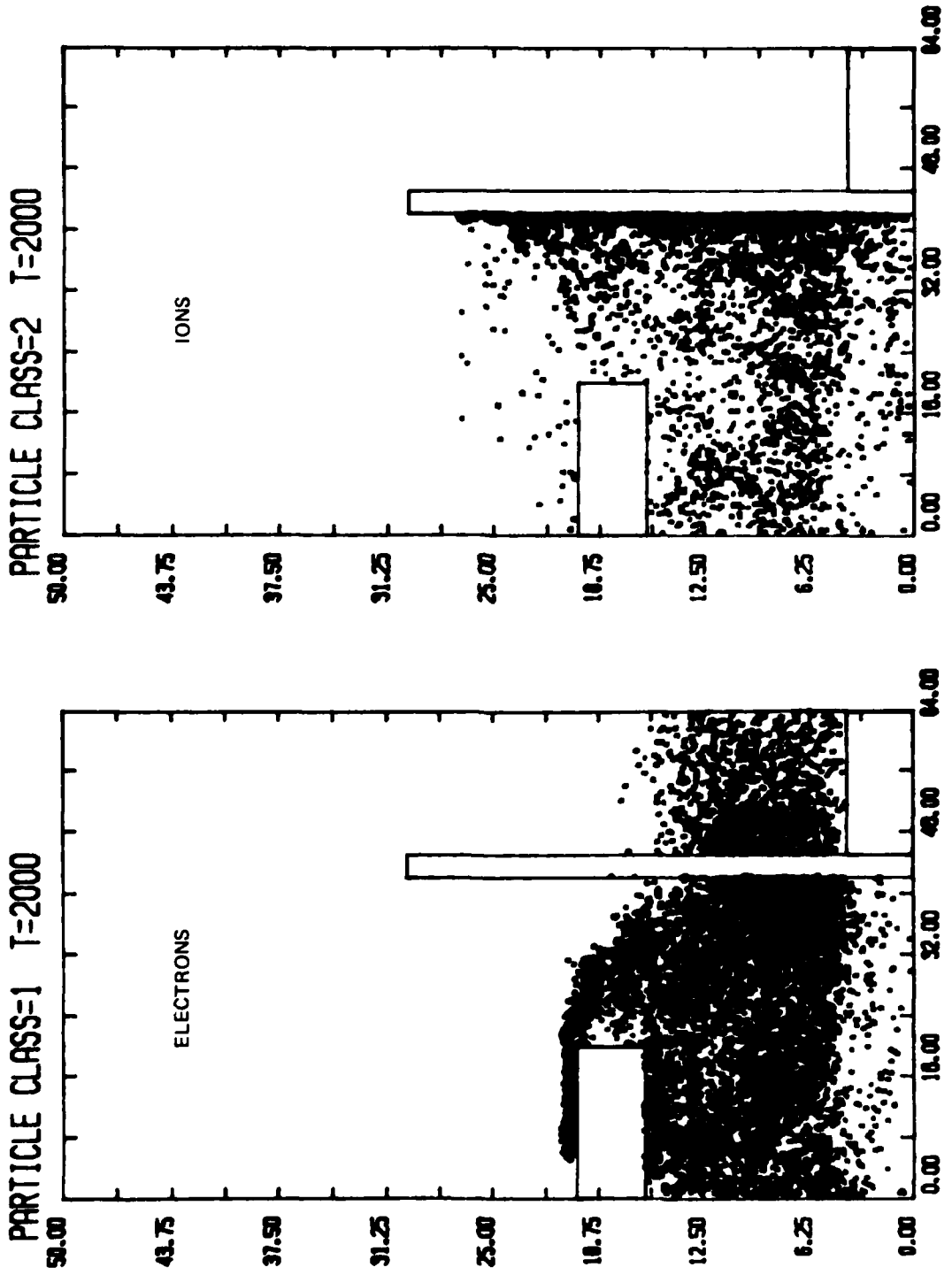

Fig. 16 — PBFA-I electron and ion flow for $J_0 = 4$ kA/cm^2

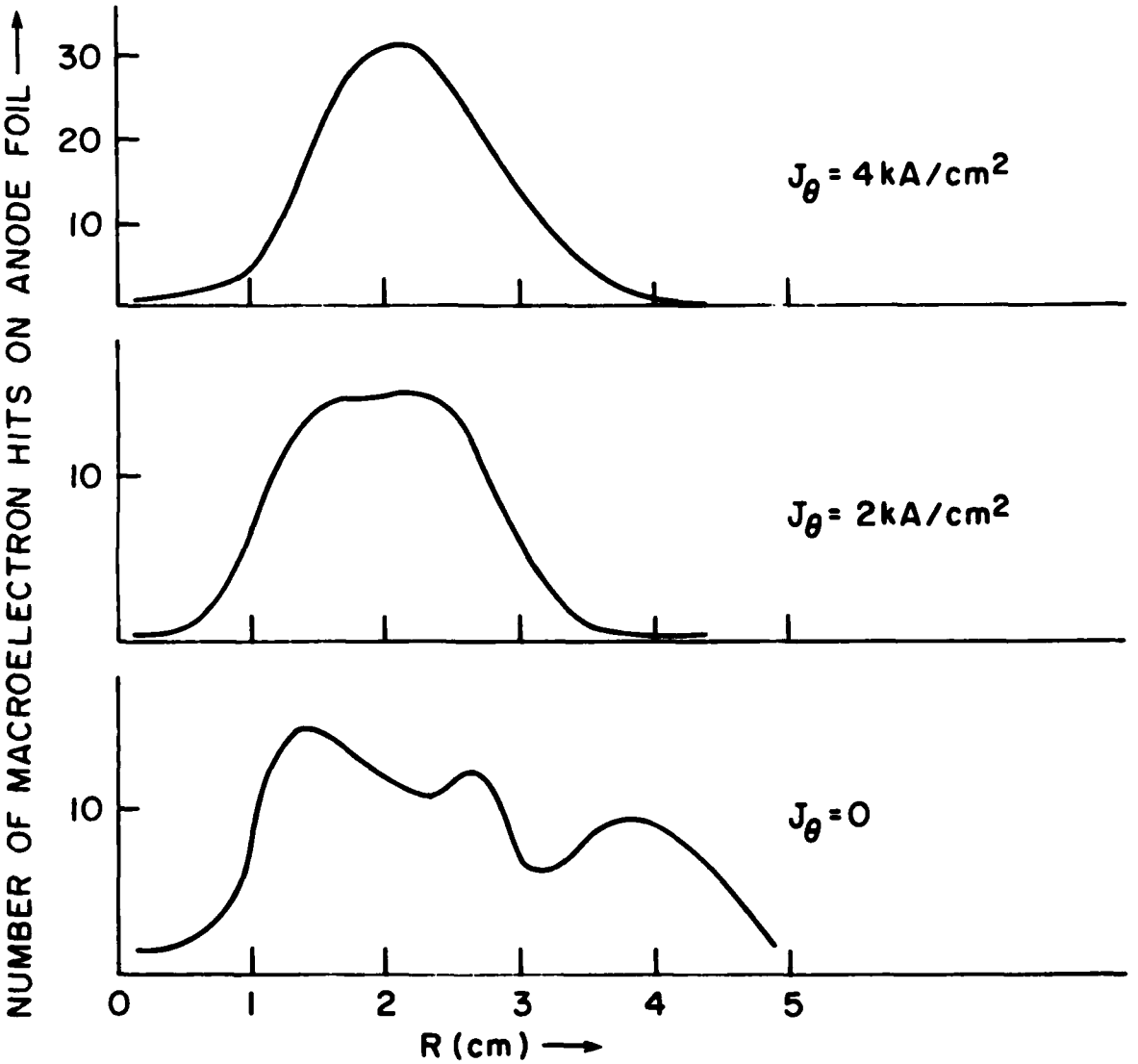

Fig. 17 — Comparative radial profiles of electron impacts on anode foil

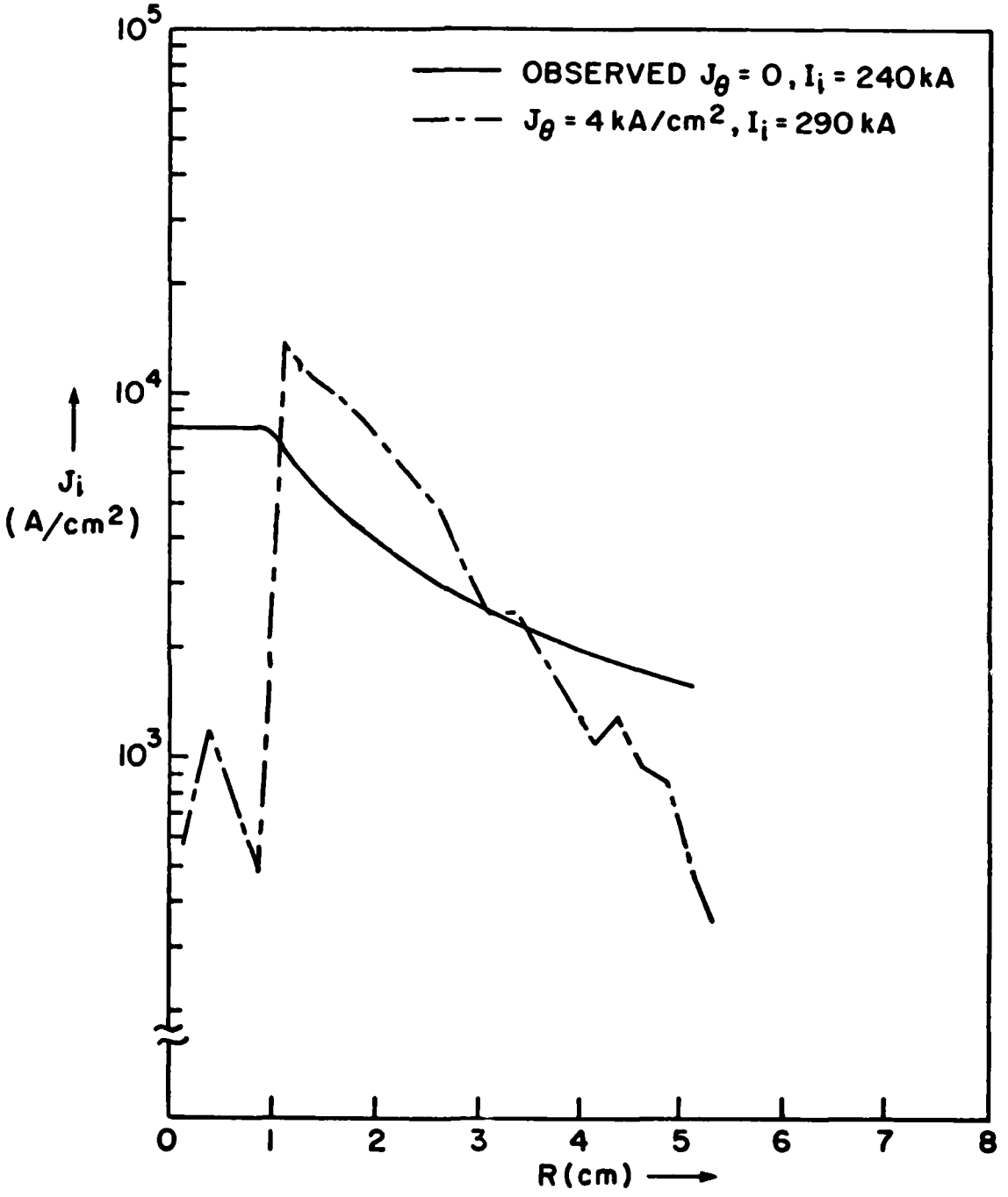

Fig. 18 — Radial profiles of PBFA-I ion current density

20% in $(\eta_i)_{effective}$ and thereby recommends this J_θ-diode for experimental testing on GAMBLE-II for possible use on PBFA.

In addition to this favorable result regarding enhanced effective ion production, several other results merit mention. Comparison of Figure 18 to the corresponding AURORA J_i profiles of Figure 11 show a hollowing of the ion beam. The central axis current density peak dissappears. Since shank electrons with their finite angular momentum cannot reach $R = 0$, this indicates that significantly more electrons are being emitted from the recessed cathode foil on the AURORA diode. These *can* reach $R = 0$ and enhance ion emission there. Another difference between the two impedance regimes is the nature of the cathode shank electron flow. On AURORA, the imposition of J_θ actually enhanced electron emission on the shank by lifting the flow away from the surface. This phenomenon does not manifest itself in the 4Ω runs. Finally, there was some question whether any actual magnetic insulation of the electron flow from the anode foil was taking place. The answer was obtained by measuring the strength of the radial component of the magnetic field one-half data cell (0.015 cm) from the magnetic-flux-excluding surface of the anode foil. Figure 19 shows that, as expected, very high fields are to be found over large areas of the foil. This is typical of the diamagnetic field enhancement observed in magnetically insulated radial diodes.[31]

IV. CONCLUSIONS

The major results of all of the above computer simulations are summarized in Table 1. The *imposition of a relatively small azimuthal current in the hollow cathode shank of a 4-ohm axial diode* has been numerically shown to increase the *effective* ion production efficiency of the diode by over 20%. This positive result recommends the further study of the new concept both theoretically and experimentally. Additional simulations should be conducted to examine diode equilibria for other values of J_θ. Experimentally, an actual J_θ-diode has been constructed as shown in Figure 20. Its cathode shank is approximately six centimeters in diameter with 48 slots 3/8 inch deep, 0.045 inch wide, and angled at 20° cut around its periphery in order to generate a J_θ by spiraling the current flowing through the

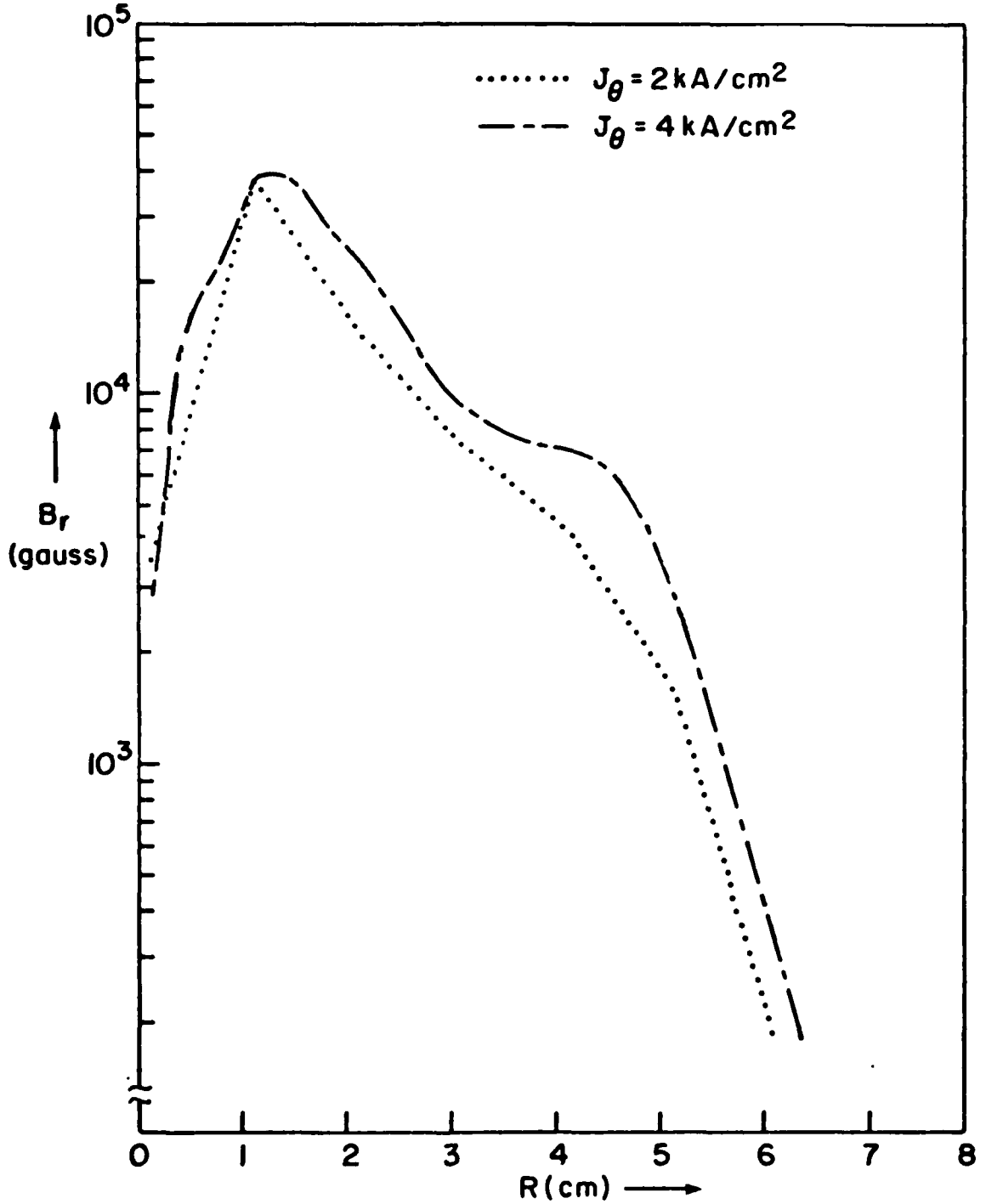

Fig. 19 — Radial profiles of B_R near PBFA-I anode foil

Table 1 – Summary of Major Results

	AURORA (5 MV)				PBFA (2 MV)	
J_θ (kA/cm^2)	0 ($^{neg.}_{pol.}$)	0 ($^{pos.}_{pol.}$)	1	4	0	4
I_e (kA)	165	182	244	257	300	322
I_i (kA)	40	56	41	34	200	232
$(I_i)_{eff}$ (kA)	35	50	35	30	150	207
I_{diode} (kA)	205	238	285	291	500	555
Z (ohms)	24.4	21.0	17.5	17.2	4.0	3.6
η_i	0.195	0.235	0.144	0.117	0.40	0.42
$(\eta_i)_{eff}$	0.171	0.210	0.123	0.103	0.30	0.37

Fig. 20 — The experimental J-Theta Diode (JTD) for testing on Gamble-II

shank. Three shots were conducted using this diode on GAMBLE-II but diagnostic difficulties prevented the gathering of enough useful information for proper evaluation. Additional shots will be attempted as circumstances permit.

For diodes with impedances in the neighborhood of twenty ohms, no evidence of ion efficiency boosting via a shank J_θ has been obtained. However, even for that case the azimuthal current component does significantly modify the radial profile of the extractable ion current density. Such a capability to change the shape of the ion beam which emerges from the diode may prove useful in the future for optimizing this beam for transport away from the diode through plasma channels.

ACKNOWLEDGMENTS

The authors are indebted to R.A. Meger and S.J. Stephanakis for their valuable assistance in the preparation of this report.

JDT REFERENCES

1. G. Cooperstein, S.A. Goldstein, D. Mosher, and R.J. Barker, et al., NRL Memo Report 4387 (1980).

2. D.J. Johnson, G.W. Kuswa, A.V. Farnsworth, Jr., and J.P. Quintenz, et al., Phys. Rev. Lett. **42**, 610 (1979).

3. G. Cooperstein, S.A. Goldstein, and D. Mosher, et al., in Proceedings 3rd International Topical Conference on High Power Electron and Ion Beam Research and Technology, Novosibirsk, USSR (1979).

4. D.J. Johnson, Bull. Am. Phys. Soc. **24**, 9[illegible] (1979).

5. S.J. Stephanakis, J.R. Boller, G. Cooperstein, S.A. Goldstein, D.D. Hinshelwood, D. Mosher, F.W. Oliphant, F. Sandel, and F.C. Young, Bull. Am. Phys. Soc. **23**, 907 (1978).

6. D.G. Colombant, S.A. Goldstein, and D. Mosher, Phys. Rev. Lett. **45**, 1253 (1980).

7. R.A. Meger, F.C. Young, G. Cooperstein, S.A. Goldstein, and D. Mosher, NRL Memo Report 4477 (1981).

8. D.J. Johnson, S.A. Goldstein, R. Lee, and W.F. Oliphant, J. Appl. Phys. **49**, 4634 (1978).

9. S.A. Goldstein and R. Lee, Phys Rev. Lett. **35**, 1079 (1975).

10. S.A. Goldstein, R.C. Davidson, J.G. Siambis, and R. Lee, Phys. Rev. Lett. **33**, 1471 (1974).

11. D.P. Bacon, S.A. Goldstein, R. Lee, and G. Cooperstein, NRL Memo Report 4326 (1980).

12. M.M. Widner, J.W. Poukey, and J.A. Halbleib, Sr., Phys. Rev. Lett. **38**, 548 (1977).

13. J.W. Shearer, Lawrence Livermore Lab Report UCRL-52129 (1976).

14. R.J. Barker and P.F. Ottinger, NRL Memo Report 4654 (1981).

15. R.J. Barker and S.A. Goldstein, to appear as an NRL Memo Report (1982).

16. R.J. Barker and S.A. Goldstein, Bull. Am. Phys. Soc. **25**, 900 (1980).

17 Suggested independently for other applications by F. Sandel in 1978.

18. S.A. Goldstein, J. Appl. Phys. **47**, 894 (1976).

19. A.E. Blaugrund, G. Cooperstein, and S.A. Goldstein, Phys. Fluids **20**, 1185 (1977).

20. D. Mosher, Bull. Am. Phys. Soc. **25**, 900 (1980).

21. J.W. Poukey, J.R. Freeman, and G. Yonas, J. Vac. Sci. Technol. **10**, 954 (1973).

22. S. Humphries, Jr., Plasma Physics **19**, 399 (1977).

23. R.J. Barker, A.T. Drobot, R. Lee, and S.A. Goldstein, Proc. 9th Conf. on the Numerical Simulation of Plasmas, Evanston, Ill. (1980).

24. R.A. Meger, A.T. Drobot, S.A. Goldstein, and F.C. Young, Bull. Am. Phys. Soc. 25, 900 (1980).

25. F.C. Young and R.A. Meger, et al., Bull. Am. Phys. Soc. 25, 899 (1980).

26. R.J. Barker, Banach Center Publications 3, 255, Warsaw, Poland (1975).

27. R.A. Meger, F.C. Young, and A.T. Drobot, et al., NRL Memo Report 4477 (1981) and J. Appl. Phys. 52, 6084 (1981).

28. S.J. Stephanakis, S.A. Goldstein, D. Mosher, and W.F. Oliphant, Bull. Am. Phys. Soc. 25, 900 (1980).

29. A.T. Drobot, private communication.

30. R.J. Barker, S.A. Goldstein, and R.E. Lee, NRL Memo Report 4279 (1980).

31. R.J. Barker, S.A. Goldstein, and A.T. Drobot, Proc. IEEE Conf. on Plasma Science, Madison, Wisc. (1980).

DISTRIBUTION LIST AUGUST 1981

Director
Defense Intelligence Agency
Washington, DC 20301

Attn: DTICI Robert I. Rubenstein 1 copy

Defense Advanced Research Project Agency
1400 Wilson Blvd.
Arlington, VA 22209
Attn: J. Bayless 1 copy

Director
Defense Nuclear Agency
Washington, DC 20305

Attn: FCPR 1 copy
STVL 1 copy
TISI Archives 1 copy
TITL Tech. Library 3 copies
J. Z. Farber (RAEV) 1 copy
R. L. Gullickson (RAEV) 1 copy

Defense Technical Information Center
Cameron Station
5010 Duke Street
Alexandria, VA 22314

Attn: T. C. 12 copies

Under Sec'y of Defense for RSCH and ENGRG
Department of Defense
Washington, DC 20301

Attn: S&SS(OS) 1 copy

Chief
Livermore Division Fld Command DNA
Lawrence National Laboratory
P. O. Box 808
Livermore, CA 94550

Attn: FCPRL 1 copy

National Technical Information Service
U.S. Department of Commerce
5285 Port Royal Road
Springfield, VA 22161 24 copies

Commander
BMD System Command
P. O. Box 1500
Huntsville, AL 35807

Attn: SSC-TEN 1 copy

DEP Chief of Staff for RSCH DEV & ACQ
Department of the Army
Washington, DC 20310

Attn: DAMA-CSM-N 1 copy

Commander
Harry Diamond Laboratories
2800 Powder Mill Road
Adelphi, MD 20783
(CNWDI-INNER ENVELOPE: ATTN: DELHD-RBH)

Attn: DELHD-NP 1 copy
DELHD-RCC J. A. Rosado 1 copy
DRXDO-RBH P. A. Caldwell 1 copy

DRXDO-TI Tech Lib. 1 copy
S. Graybill 1 copy

Commander
Picatinny Arsenal
Dover, NJ 07801

Attn: SMUPA ND-N-E 1 copy

U. S. Air Force Office of Scientific Research
Physics Directorate
Bolling A.F.B., DC 20332

Attn: A. K. Hyder 1 copy
M. A. Stroscio 1 copy

Commander
U. S. Army Missile Command
Redstone Arsenal, AK 35809

Attn: Redstone Scientific Information CTR
DRCPM-PM-PE-EA 1 copy

Commander
U. S. Army Nuclear Agency
7500 Backlick Road
Building 2073
Springfield, VA 22150

Attn: ATCN-W 1 copy

Commander
U. S. Army Test and Evaluation COMD
Aberdeen Proving Ground, MD 21005

Attn: DRSTE-EL 1 copy

Commander
Naval Electronic Systems CMD HQS
Washington, DC 20360

Attn: Code 5032 1 copy

Commanding Officer
Naval Intelligence Support Center
4301 Suitland Road - Building 5
Washington, DC 20390

Attn: NISC-45 1 copy

Naval Research Laboratory

Addressee: Attn: Name/Code	
Code 2628 - TIC-Distribution	25 copies
Code 4040 - J. Boris	1 copy
Code 6682 - D. Nagel	1 copy
Code 4700 - S. Ossakow	26 copies
Code 4707 - J. Davis	1 copy
Code 4730 - S. Bodner	1 copy
Code 4740 - V. Granatstein	1 copy
Code 4760 - B. Robson	1 copy
Code 4761 - C. Kapetanakos	1 copy
Code 4770 - Branch Head	10 copies
Code 4770 - F. Young	1 copy
Code 4770 - S. Stephanakis	1 copy
Code 4771 - D. Mosher	10 copies
Code 4773 - G. Cooperstein	10 copies
Code 4790 - D. Colombant	1 copy
Code 4790 - I. Haber	1 copy
Code 4790 - M. Lampe	1 copy
On-Site Contractors:	
Code 4770 - R. Barker (Jaycor)	25 copies
Code 4770 - S. Goldstein (Jaycor)	10 copies
Code 4770 - R. Meger (Jaycor)	1 copy
Code 4770 - P. Ottinger (Jaycor)	1 copy
Code 4770 - F. Sandel (Jaycor)	1 copy
Code 4790 - A. Drobot (SAI)	1 copy

Officer-in-Charge
Naval Surface Weapons Center
White Oak, Silver Spring, MD 20910

Attn:	
Code WR43	1 copy
Code WA501 - Navy Nuc Prgms Off	1 copy

Chief of Naval Operations
Navy Department
Washington, DC 20350

Attn: R. A. Blaise 604C4 — 1 copy

Commander
Naval Weapons Center
China Lake, CA 93555

Attn: Code 533 Tech Lib. — 1 copy

AF Weapons Laboratory, AFSC
Kirtland AFB, NM 87117

Attn:	
CA	1 copy
ELC	1 copy
NT	1 copy
SUL	1 copy
DYP	1 copy
J. Darrah	1 copy
W.L. Baker	1 copy

HQ USAF/RD
Washington, DC 20330

Attn: RDQSM — 1 copy

Director
Joint Strat TGT Planning Staff JCS
OFFUTT AFB
Omaha, NB 68113

Attn: JSAS — 1 copy

SAMSO/DY
Post Office Box 92960
Worldway Postal Center
Los Angeles, CA 90009
(Technology)

Attn: DYS — 1 copy

SAMSO/IN
Post Office Box 92960
Worldway Postal Center
Los Angeles, CA 90009

Attn: IND MAJ D. S. Muskin — 1 copy

SAMSO/MN
Norton AFB, CA 92409
(Minuteman)

Attn: MNNH — 1 copy

SAMSO/SK
Post Office Box 92960
Worldway Postal Center
Los Angeles, CA 90009
(Space Comm Systems)

Attn: SKF P. H. Stadler — 1 copy

U. S. Department of Energy
Division of Inertial Fusion
Washington, DC 20545

Attn:	
G. Canavan	1 copy
T. F. Godlove	1 copy
S. L. Kahalas	1 copy
R. L. Schriever	1 copy

U.S. Department of Energy
P.O. Box 62
Oak Ridge, TN 37830 — 50 copies

Argonne National Laboratory
9700 South Cass Avenue
Argonne, Illinois 60439

Attn:	
G. R. Magelssen	1 copy
R. J. Martin	1 copy

Brookhaven National Laboratory
Upton, NY 11973

Attn: A.F. Maschke — 1 copy

Lawrence Berkley Laboratory
Berkeley, CA 94720

Attn: D. Keefe — 1 copy

Lawrence Livermore National Laboratory
P. O. Box 808
Livermore, CA 94550

Attn:	L-18	1 copy
	L-153	1 copy
	R. J. Briggs	1 copy
	E. P. Lee	1 copy
	J. H. Nuckolls	1 copy
	S. S. Yu	1 copy
	Tech Info Dept. L-3	1 copy
	D.J. Meeker	1 copy
	A.B. Langdon	1 copy
	E. Teller	1 copy
	D.S. Prono	1 copy

Los Alamos National Laboratory
P. O. Box 1663
Los Alamos, NM 87545

Attn:	D. B. Henderson	1 copy
	R. B. Perkins	1 copy
	L. E. Thode	1 copy
	C. Barnes	1 copy
	D. Forslund	1 copy
	R.O. Bangerter	1 copy
	W.P. Gula	1 copy

National Science Foundation
Mail Stop 19
Washington, DC 20550

Attn: D. Berley 1 copy

Sandia National Laboratories
P. O. Box 5800
Albuquerque, NM 87185

Attn:	J. R. Freeman / 4241	1 copy
	S. Humphries / 4253	1 copy
	D. J. Johnson / 4244	1 copy
	G. W. Kuswa / 4240	1 copy
	P. A. Miller / 4244	1 copy
	J. P. Vandevender / 4252	1 copy
	G. Yonas / 4200	1 copy
	Doc Con for 3141 Sandia RPT Coll	1 copy
	J.N. Olsen / 4244	1 copy
	G.A. Allshouse / 4247	1 copy
	T.A. Mehlhorn / 4247	1 copy
	M.M. Widner / 4247	1 copy
	T.P. Wright / 4241	1 copy
	J.P. Quintenz / 4241	1 copy
	P.L. Mix / 4242	1 copy
	C.W. Mendel /4244	1 copy
	A.V. Farnsworth / 4247	1 copy
	M.A. Sweeney / 4247	1 copy
	D.B. Seidel / 4241	1 copy

AVCO Research and Systems Group
201 Lowell Street
Wilmington, MA 01887

Attn: Research Lib. A830 Rm. 7201 1 copy

BDM Corporation, The
795 Jones Branch Drive
McLean, VA 22101

Attn: Tech Lib. 1 copy

Bechtel Group, Inc.
P.O. Box 3965
San Francisco, CA 94119

Attn: W. O. Allen 1 copy

Boeing Company, The
P. O. Box 3707
Seattle, WA 98124

Attn: Aerospace Library 1 copy

Cornell University
Ithaca, NY 14850

Attn:	D. A. Hammer	1 copy
	R. N. Sudan	1 copy
	J. Maenchen	1 copy
	J.B. Greenley	1 copy
	C.B. Wharton	1 copy

The Dikewood Corporation
1613 University Blvd., NE
Alburquerque, NM 87102

Attn: L. Wayne Davis 1 copy

EG&G, Inc.
Albuquerque Division
P. O. Box 10218
Albuquerque, NM 87114

Attn: Technical Library 1 copy

Electric Power Research Institute
3412 Hillview Avenue
P.O. Box 10412
Palo Alto, CA 94303

Attn: K.W. Billman 1 copy

Ford Aerospace & Communications Operations
Ford & Jamboree Roads
Newport Beach, CA 92663
(Formerly Aeronutronic Ford Corporation)

Attn: Tech Info Section 1 copy

General Electric Company
Space Division
Valley Forge Space Center
Goddard Blvd., King of Prussia
P. O. Box 8555
Philadelphia, PA 19101

Attn: J. C. Penden VFSC, Rm. 4230M 1 copy

General Electric Company
Tempo-Center for Advanced Studies
816 State Street (P. O. Drawer QQ)
Santa Barbara, CA 93102

Attn: DASIAC 1 copy

Grumman Aerospace Corporation
Bethpage, NY 11714

Attn: P. Suh — 1 copy

Institute for Defense Analyses
400 Army-Navy Drive
Arlington, VA 22202

Attn: IDA Librarian R S. Smith — 1 copy

Ion Physics Corporation
South Beford Street
Burlington, MA 01803

Attn: H. Milde — 1 copy

IRT Corporation
P. O. Box 81087
San Diego, CA 92138

Attn: R. L. Mertz — 1 copy

JAYCOR, Inc.
205 S. Whiting Street
Alexandria, VA 22304

Attn: E. Alcaraz — 1 copy
J. Guillory — 1 copy
R. Hubbard — 1 copy
R. Sullivan — 1 copy
D. A. Tidman — 1 copy

JAYCOR, Inc.
11011 Torreyana Road
San Diego, CA 92121

Attn: E. Wenaas — 1 copy
S.S. Wang — 1 copy

Kaman Science Corporation
P. O. Box 7463
Colorado Springs, CO 80933

Attn: A. P. Bridges — 1 copy
D. H. Bryce — 1 copy
J. R. Hoffman — 1 copy
W. E. Ware — 1 copy

Lockheed Missiles and Space Co., Inc.
3251 Hanover Street
Palo Alto, CA 94304

Attn: L. F. Chase — 1 copy

Massachusetts Institute of Technology
Cambridge, MA. 02139

Attn: R.C. Davidson — 1 copy
G. Bekefi — 1 copy
D. Hinshelwood — 1 copy

Maxwell Laboratories, Inc.
9244 Balboa Avenue
San Diego, CA 92123

Attn: R. W. Clark — 1 copy
A. C. Kolb — 1 copy
P. Korn — 1 copy
A. R. Miller — 1 copy
J. Pearlman — 1 copy
J. Shannon — 1 copy

McDonnell Douglas Corporation
5301 Bolsa Avenue
Huntington Beach, CA 92647

Attn: S. Schneider — 1 copy

Mission Research Corporation
1400 San Mateo Blvd. SE
Albuquerque, NM 87108

Attn: B. B. Godfrey — 1 copy

Mission Research Corporation-San Diego
P. O. Box 1209
LaJolla, CA 92038

Attn: V.A.J. Van Lint — 1 copy

Mission Research Corporation
735 State Street
Santa Barbara, CA 93101

Attn: W. C. Hart — 1 copy
C. L. Longmire — 1 copy

Northrop Corporation
Electronic Division
2301 West 120th Street
Hawthorne, CA 90250

Attn: V. R. DeMartino — 1 copy

Northrop Corporation
Northrop Research and Technology Ctr.
3401 West Broadway
Hawthorne, CA 90205 — 1 copy

Physical Dynamics
P.O. Box 556
La Jolla, CA 92037

Attn: S. Jorna — 1 copy

Physics International Co.
2700 Merced Street
San Leandro, CA 94577

Attn: J. Benford — 1 copy
B. Bernstein — 1 copy
G. Frazier — 1 copy
E. B. Goldman — 1 copy
R. Huff — 1 copy
A. J. Toepfer — 1 copy
G. Dahlbacka — 1 copy

Power Conversion Technology, Inc.
1158 Sorrento Vally Road
San Deigo, CA 92121

Attn: V. Fargo — 1 copy
D.A. Phelps — 1 copy

Princeton Plasma Physics Laboratory
James Forrestal Campus
P.O. Box 451
Princeton, N.J. 08540

Attn: R. Kulsrud — 1 copy

Pulse Sciences, Inc.
1615 Broadway, Suite 610
Oakland, CA 94612

Attn: I. Smith — 1 copy
P. Spence — 1 copy
S. Putnam — 1 copy

R&D Associates
P. O. Box 9695
Marina Del Rey, CA 90291

Attn: W. R. Graham, Jr. — 1 copy
M. Grover — 1 copy
C. MacDonald — 1 copy
E. Martinelli — 1 copy

R&D Associates
Suite 500
1401 Wilson Blvd.
Arlington, VA 22209

Attn: P. J. Turchi — 1 copy

Science Applications, Inc.
P. O. Box 2351
LaJolla, CA 92038

Attn: J. Robert Beyster — 1 copy

Spire Corporation
P. O. Box D
Bedford, MA 01730

Attn: R. G. Little — 1 copy

SRI International
333 Ravenswood Avenue
Menlo Park, CA 94025

Attn: S. Ddairiki — 1 copy
R.J. Vidmar — 1 copy

Stanford University
SLAC
P. O. Box 4349
Stanford, CA 94305

Attn: W. B. Herrmannsfeldt — 1 copy

Systems, Science and Software, Inc.
P. O. Box 1620
LaJolla, CA 92038

Attn: A. R. Wilson — 1 copy

Texas Tech University
P. O. Box 5404 North College Station
Lubbock, TX 79417

Attn: T. L. Simpson — 1 copy
M. Kristiansen — 1 copy

TRW Defense and Space Sys Group
One Space Park
Redondo Beach, CA 90278

Attn: Tech Info Center/S-1930 — 1 copy
Z.G.T. Guiragossian — 1 copy
D. Arnush — 1 copy

University of California
Dept. of Physics
La Jolla, CA 92037

Attn: K. Brueckner — 1 copy
W.B. Thompson — 1 copy

University of California
Boelter Hall 7731
Los Angeles, CA 90024

Attn: F.F. Chen — 1 copy

University of California
Irvine, CA 92717

Attn: G. Benford — 1 copy
N. Rostoker — 1 copy
S. Robertson — 1 copy
A. Fisher — 1 copy

University of Illinois
Urbana, IL 61801

Attn: G. H. Miley — 1 copy
J. T. Verdeyen — 1 copy

University of Rochester
Laboratory of Laser Energetics
River Station, Hopeman 110
Rochester, NY 14627

Attn: Director — 1 copy

University of Scranton
Dept. of Physics
Scranton, PA 18510

Attn: F. Murray — 1 copy

Univ. of Washington
Dept. of Nuclear Engineering
BF-10
Seattle, WA 98115

Attn: F. Ribe — 1 copy

Univ. of Wisconsin
Dept. of Nuclear Engineering
1500 Johnson Drive
Madison, WI 53706

Attn: G.A. Moses — 1 copy
G.L. Kulcinski — 1 copy

Vought Corporation
Michigan Division
38111 Van Dyke Road
Sterling Heights, MI 48077
(Formerly LTV Aerospace Corp)

Attn: Tech Lib — 1 copy

Westinghouse Electric Corporation
Research and Development Center
1310 Beulah Road
Pittsburgh, PA 15235

Attn: M.D. Nahemow — 1 copy

Atomic Weapons Research Establishment
Building H36
Aldermaston, Reading RG 7 4PR
United Kingdom

Attn: J. C. Martin — 1 copy

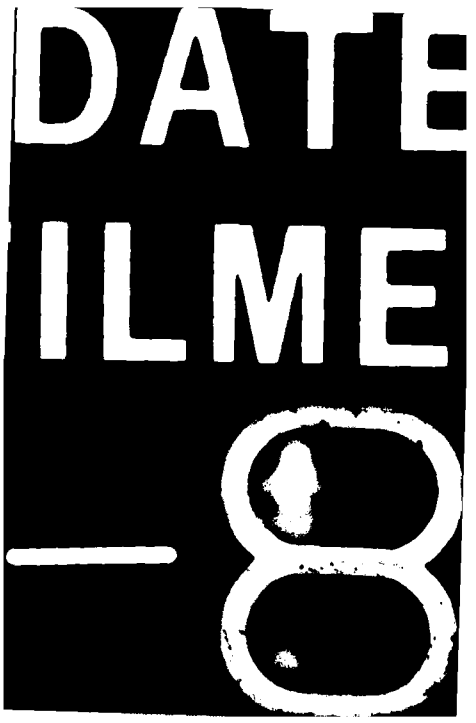
DATE:
ILME
8